Check for updates

Received: 27 May 2020 | Revised: 4 November 2020 | Accepted: 8 January 2021

DOI: 10.1002/aic.17228

REACTION ENGINEERING, KINETICS AND CATALYSIS

AIChE JOURNAL

# Taylor-Couette reactor: Principles, design, and applications

Marco Schrimpf[1] | Jesús Esteban[1,2] | Helge Warmeling[3] | Tobias Färber[3] | Arno Behr[3] | Andreas J. Vorholt[1]

[1]Molecular Catalysis, Max Planck Institute for Chemical Energy Conversion, Mülheim an der Ruhr, Germany

[2]Department of Chemical Engineering and Analytical Science, School of Engineering, The University of Manchester, Manchester, United Kingdom

[3]Department of Biochemical and Chemical Engineering, Chair of Technical Chemistry, Technical University of Dortmund, Dortmund, Germany

**Correspondence**
Andreas J. Vorholt, Max Planck Institute for Chemical Energy Conversion, Mülheim an der Ruhr, Germany.
Email: andreas-j.vorholt@cec.mpg.de

## Abstract

The Taylor-Couette reactor (TCR) is an apparatus that capitalizes on the Taylor-Couette flow, which allows many flow regimes and conditions to perform (bio-)chemical conversions with precise control of various reactor characteristics. With the possibility to continuously perfuse the reactor with a reaction medium, the TCR becomes interesting for chemical engineering applications. In this review, we introduce this reactor type and provide an overview of its history, principles of the flow regimes, and a description and design aspects of the reactors and their elements. Available information in the literature is summarized and harmonized to present available formulas and correlations in a consistent set of variables. Additionally, a wide number of applications in process technology are covered, including reactions in homogeneous, photo, and enzymatic catalysis, polymer synthesis, and crystallization and aggregation-flocculation processes. Focusing on this reactor configuration, this article intends to be used as a hub for scientific groups interested in TCRs.

**KEYWORDS**
crystallization, heat and mass transfer, photocatalysis, reactor design, Taylor flow

## 1 | INTRODUCTION

Process technology applications demand enhanced heat and mass transfer, higher performance leading to better overall reaction rates, yields and selectivity to the desired products and as well as controlled flow for varying throughput while minimizing the costs. Thus, multiple investigations on reactor configurations have arisen to intensify the mixing. Various reviews cover intensified reactors such as fluidic oscillators based on the Coanda effect,[1] oscillatory baffled reactors,[2] devices to cause hydrodynamic cavitation[3] or a range of pulsating flows by ultrasound or mechanical vibration,[4] static mixer reactors,[5] microreactors,[5-7] and ejector loop reactors.[5,8] Reactors based on the Taylor-Couette flow (Taylor-Couette reactors, TCRs) however are considered more scarcely, with the available reviews focusing more on the flow itself rather than the apparatus and its technical applications.

Historically, in 1888 Mallock was the first to report the flow behavior between rotating cylinders.[9,10] Couette later systematically described the classic Couette flow at low levels of turbulence, where a fluid is dragged between two plates of whom one is moving.[11] Later, in 1923, Geoffrey I. Taylor theoretically and experimentally investigated the formation of counter-rotating stable vortices in the gap between a rotating cylinder and the shell at increasing turbulence levels.[12] Since the middle of the 20th century, flow patterns occurring at higher turbulence levels were investigated as well.[13-17] However, these investigations focused solely on the flow phenomenon. With the publication of Kataoka et al., investigations emerged that paid special attention to the ability of the Taylor-Couette flow to approach plug-flow behavior.[18,19] Soon, starting with Gu et al. and Moore et al., other groups began started to devise their studies specifically for reactor design purposes, focusing more on the numerical simulation based on the observation of the vortex formation and axial dispersion.[20,21] The Taylor-Couette reactor (TCR) was born. For further reading, a more exhaustive review on these turbulent early days of the flow type was released by Donnelly in 1991.[22]

The standard TCR consists of a cylindrical shell in which a rotating inner cylinder is inserted so that an annular gap is formed. Various

This is an open access article under the terms of the Creative Commons Attribution-NonCommercial-NoDerivs License, which permits use and distribution in any medium, provided the original work is properly cited, the use is non-commercial and no modifications or adaptations are made.
© 2021 The Authors. *AIChE Journal* published by Wiley Periodicals LLC. on behalf of American Institute of Chemical Engineers.

flow regimes can be formed in the annular gap, resulting in significantly different flow conditions and shapes. The mixing conditions in a Taylor-Couette reactor can be set nearly independently from the axial flow by changing the rotational speed of the cylinders as well as the geometry of the reactor itself. The flow regime can hence be tailored specifically to the demand of the process—from mixing and dispersing due to high shear forces to high flow segregation resulting in a plug-flow behavior.[18,19] However, while this is interesting for a wide range of applications in process technology, studies targeting process dynamics and control in continuous systems are yet to come.[23] Further, a lack of reports on industrial applications indicates that the TCR is, as yet, still limited by its complex design and operation, and difficult scale-up.

Among others, academic applications of these reactor setups include studies covering homogeneous transition metal catalysis, photocatalytic, and enzymatic reactions, polymer synthesis and solid processing operations like crystallization reactions or aggregation-flocculation. Further applications or occurrences of the apparatus include separation processes like blood plasma filtrations[24] or different liquid–liquid mixing and separations such as extraction.[25-28]

With the Taylor-Couette flow having been covered in the past,[29,30] this review first gives an understanding of the fundamental phenomena of the flow, the engineering aspects relevant to reactor design, finally an overview of applications using this reactor setup. In this sense, not the Taylor-Couette flow is the focus of this review, but the apparatus that is the Taylor-Couette reactor.

## 2 | FUNDAMENTALS OF TAYLOR-COUETTE FLOW

Before discussing the TCR, a solid understanding of the underlying phenomena is necessary to evaluate applications and recent advances of this reactor. In this sense, the most important phenomena are the attainable flow regimes, for which the characteristic number used is the Taylor number *Ta*, also referred to as the cylinder Reynolds number $Re_{cyl}$. In general, it relates centrifugal to the viscous forces, meaning that growing values correspond to higher levels of turbulence. Different definitions for *Ta* exist in literature and an overview of common definitions is given in Table 1.[12,14,29,31-38] For the sake of brevity, in this work the definition in Equation (1) is based on the definition given by Lueptow et al.[35,39] and Richter et al.[35] that equals *Ta* to $Re_{cyl}$. Hence, the presented equations are harmonized following this definition. Another important dimensionless number is the axial Reynolds number $Re_{ax}$ as defined in Equation (2).

$$Ta = Re_{cyl} = \frac{\omega \cdot r_i \cdot d}{\nu} \tag{1}$$

$$Re_{ax} = \frac{u_{ax} \cdot d}{\nu} \tag{2}$$

Regardless of the different existing definitions, *Ta* is determined by geometric proportions like the gap width *d*, the diameter of the inner cylinder $d_i$, the angular velocity $\omega$ as well as fluid properties like kinematic viscosity $\nu$. $Re_{ax}$ further depends on the axial velocity $u_{ax}$.

The flow regimes in the annular gap vary with $\omega$ and can be characterized in terms of turbulence and the type and shape of the forming vortices. As in the case of *Ta*, the definition and naming of the prevailing flow regimes is inconsistent in literature,[39,40] but an exhaustive discussion goes beyond the focus of this review. Instead, the following paragraph focuses on flow regimes important to the application for chemical or biochemical reactors with a fixed shell. At low *Ta*, a laminar azimuthal flow regime (Couette flow) is formed, where the fluid is partly dragged through the cylinder walls.[11] Figure 1 illustrates the Couette flow for a system with a moving inner cylinder and a fixed shell. Beginning from the inner cylinder and owing to viscous forces caused by inner friction, the resulting fluid velocity profile consists of a series of concentric layers that decrease in velocity. With the addition of an axial flow, a helical flow pattern forms over the cylinder height depending on $Re_{ax}$.

When $\omega$ is increased, impartial to whether the flow is superimposed by an axial flow, a centrifugal instability sets in that initiates the formation of toroidal vortices and the flow transforms into the Taylor-vortex flow. This flow regime, also referred to as the Taylor-Couette flow, is characterized by symmetrical counter-rotating toroidal vortices, as illustrated in Figure 2.[41]

The point at which this transition takes place is characterized by the first critical Taylor number $Ta_{c1}$.[35]. Here, the fluid transfer

**TABLE 1** Overview of various definitions of the Taylor number found in literature

| Definition | Reference |
|---|---|
| $Re_{cyl} = \frac{d r_i \omega}{\nu}$ | 14,31-33 |
| $Ta = \frac{d r_i \omega}{\nu}$ | 34, 35 |
| $Ta = \frac{d r_i \omega}{\nu} \cdot \left(\frac{d}{r_i}\right)^{\frac{1}{2}}$ | 12, 29, 36 |
| $Ta = \left(\frac{d r_i \omega}{\nu}\right)^2 \cdot \frac{d}{r_i}$ | 37, 38 |
| $Ta = \frac{2\omega^2 d^4 \left(\eta^2 - \mu\right)}{(1-\eta^2)\nu^2}$ | 14 |

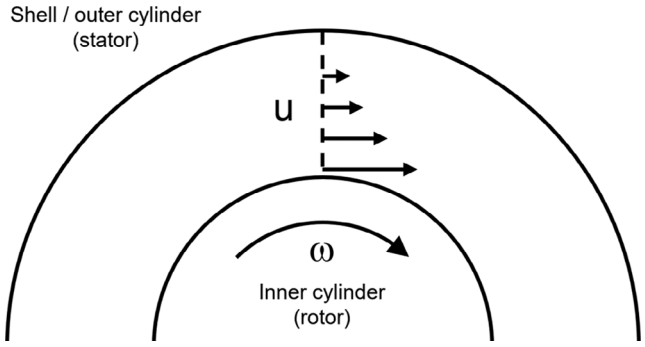


**FIGURE 1** Couette flow at low levels of turbulence in a system with an inner cylinder rotating with the angular speed $\omega$ and a fixed shell. *u* represents the resulting fluid velocity

15475905, 2021, 5, Downloaded from https://aiche.onlinelibrary.wiley.com/doi/10.1002/aic.17228, Wiley Online Library on [09/07/2024]. See the Terms and Conditions (https://onlinelibrary.wiley.com/terms-and-conditions) on Wiley Online Library for rules of use; OA articles are governed by the applicable Creative Commons License

between the individual vortices is limited, but each vortex is well mixed. While, depending on the flow conditions, the vortices may move downstream, axial dispersion models are typically used to describe the fluid transfer in the apparatus.[42] At moderate $Re_{ax}$, the vortices will be displaced without a change in their structure while at higher $u_{ax}$ a helical distortion occurs.[35,39] An increase in $Ta$ increases the inter-vortex mixing, and the axial displacement of the vortices is slowed.[42]

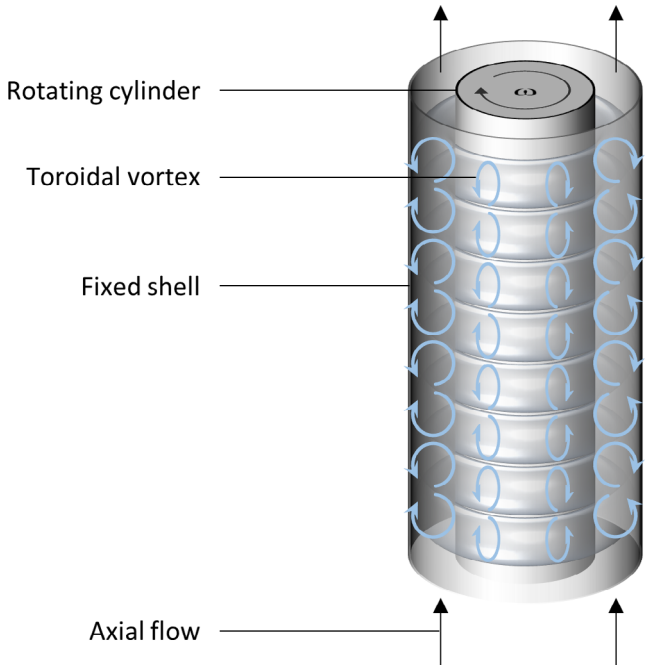


**FIGURE 2** Scheme of the toroidal vortices formed in a Taylor-Couette flow [Color figure can be viewed at wileyonlinelibrary.com]

Figure 3 shows the transition of the flow with increasing $Ta$. Increasing $Ta$ to the second critical Taylor number $Ta_{c2}$ first leads to oscillating vortices ("wavy vortex flow", [b]).[15] Past the third critical Taylor number $Ta_{c3}$, the vortices' wave amplitude becomes modulated and the flow is increasingly superimposed by a turbulent flow ("modulated wavy vortex flow." [c]).[33,43] Increasing $Ta$ further, more turbulent spots appear until full turbulence is reached (d). It must be noted that this is a simple representation of the route to turbulence that covers the most common flow patterns encountered in the TCR. In process technology, the Taylor vortex flow (a) is of great interest, as it combines excellent mixing properties with limited back mixing. Nevertheless, more flow patterns have been discovered, especially when a rotating shell is considered. For a more exhaustive review on the flow patterns, it is referred to Fardin et al.[29] Figure 3 further illustrates the equilibrium location of neutrally buoyant particles during the transition of the Taylor-Couette flow to the wavy vortex flow with increasing $Ta$.[31] While in the Taylor vortex flow the toroidal flow pattern with increasing $Ta$ is made visible with this technique (see Figure 3a), the azimuthal waves in the wavy vortex flow give insufficient time for the particles to reach the equilibrium location (see Figure 3b).

When designing a TCR, the numerical value of the critical Taylor numbers is of interest. $Ta_{c1}$ is commonly approximated by Equation (4) following the well-known publication of Taylor from 1923,[12,29] wherein $\Lambda = d_i/d_o$ denotes the diameter ratio of the TCR. A more

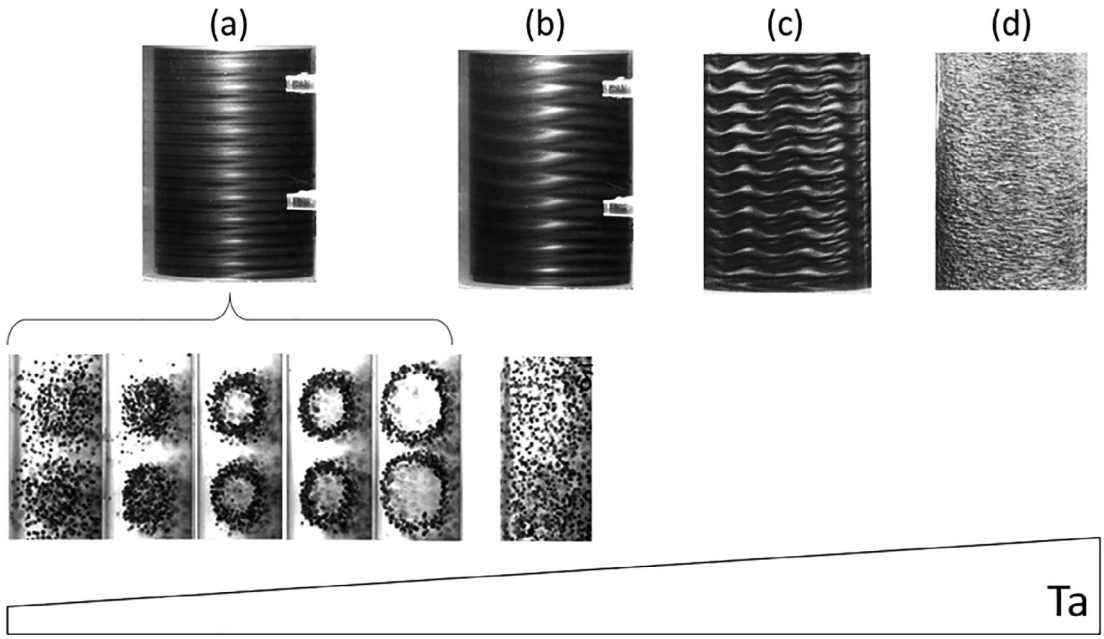


**FIGURE 3** Transition through the major flow types in a Taylor-Couette reactor and equilibrium locations of neutrally buoyant particles with growing Taylor number. (a) Taylor-vortex flow, (b) Wavy vortex flow, (c) modulated wavy vortex flow, (d) turbulent flow. Images for (a) and (b) captured by Majji and Morris (edited for increased simplicity).[31] Reproduced with permission from AIP Publishing. Copyright 2018. Pictures for (c) and (d) taken by Andereck.[14] Reproduced with permission from Cambridge University Press. Copyright 2006

15475905, 2021, 5, Downloaded from https://aiche.onlinelibrary.wiley.com/doi/10.1002/aic.17228, Wiley Online Library on [09/07/2024]. See the Terms and Conditions (https://onlinelibrary.wiley.com/terms-and-conditions) on Wiley Online Library for rules of use; OA articles are governed by the applicable Creative Commons License

accurate expression for $Ta_{c1}$ is given by Esser and Grossmann, who analytically derived the formula given in Equation (5).[44]

$$Ta_{c1} = 41.2 \cdot \sqrt{\frac{\Lambda}{1-\Lambda}} \tag{3}$$

$$Ta_{c1} = \frac{1}{0.1556^2} \cdot \frac{(1+\Lambda)^2}{2\Lambda\sqrt{(1-\Lambda)(3+\Lambda)}} \tag{4}$$

To consider the influence of axial flow on the stability, Recktenwald et al. studied the Taylor-Couette flow in a numerical stability analysis and, among other quantities, give a table listing coefficients to estimate $Ta_{c1}$ using $Re_{ax}$ and the diameter ratio as expressed in Table 2 and Equation (5).[45]

Table 3 further gives experimentally derived values for the critical Taylor numbers reported as in literature.

Most studies of the TCR for reactive systems focus on Newtonian fluids, as it is difficult to obtain Reynolds numbers for shear-thinning fluids with a distribution of viscosity.[46] However, such fluids appear in food processing, bioprocesses, and polymerization processes. The use of non-Newtonian fluids in the Taylor-Couette flow has a significant effect on the resulting flow pattern, as the mechanism of the instability and the transition to turbulence can be influenced by the nonlinearity of the fluid's rheology.[47] While the mechanism of instability of the Couette-flow are the same as for Newtonian fluids, the distribution of viscosity and modification of the azimuthal velocity profile alter the critical conditions.[48] Using a laser Doppler anemometer to measure a change in the axial velocity component, Escudier et al. found that while the transition to the Taylor-vortex flow is sharp in Newtonian fluids, it is gradual for non-Newtonian fluids,[49] further aggravating the experimental determination of the critical Taylor number. In the literature the rheology of non-Newtonian fluids is often mathematically described using the power law or the Carreau model. The critical Taylor number on the other hand is derived using various approaches. While the use of the inner wall-shear viscosity leads to a delay in the appearance of Taylor vortices corresponding to a higher $Ta_{c1}$, the use of the zero-shear viscosity leads to lowered critical Taylor numbers as the shear-thinning increases.[48] However at very strong shear-thinning, $Ta_{c1}$ may also be increased.[49] Bahrani et al. found that in comparison to Newtonian fluids an increased shear-thinning lowers the second critical Taylor number $Ta_{c2}$ at which the Taylor-vortex flow becomes unstable.[47] Cagney et al. on the other hand found that while $Ta_{c1}$ was decreased for shear-thinning fluids, for $Ta_{c2}$ no general trend was found when testing different non-Newtonian fluids.[50] Recently, Masuda et al. proposed to use an averaged viscosity weighted by the strain-rate squared and found that for small gaps with $\Lambda < 0.71$, $Ta_{c1}$ then corresponds to the theoretical value for Newtonian fluids.[46]

Concerning the flow field and the form of the vortices, several authors found that in shear-thinning fluids the following can be observed[48-52]:

- The location of the vortex eye is radially shifted against the inner cylinder wall
- Shear-thinning causes an increase in the axial wavelength of the Taylor-vortex flow
- The vortices undergo an axial drift

Escudier et al. found that for non-Newtonian fluids that are viscoelastic, the axial drift occurs in the direction opposite to the center body rotation vector.[49] Using a thixotropic fluid on the other hand caused an axial drift in the other direction. However, Cagney et al. concluded that viscoelasticity is not the dominant rheological feature that causes the drift as it can also be observed with fluids that have a low viscoelasticity and as the drift also occurs when other elastic-controlled

**TABLE 2** Correlation given by Recktenwald et al. for the estimation of $Ta_{c1}$ in the range of $0 \leq Re_{ax} \leq 20$ based on design parameters of the TCR[45]

| $\Lambda = r_i/r_o \rightarrow$ | 0.1 | 0.2 | 0.3 | 0.4 | 0.5 | 0.6 | 0.7 | 0.738 | 0.75 | 0.8 | 0.9 | 0.975 |
|---|---|---|---|---|---|---|---|---|---|---|---|---|
| Coefficients ↓ | $Ta_{c1}^2 \cdot \frac{1-\Lambda}{\Lambda} = a_0\left(1+\left(\frac{Re_{ax}}{a_2}\right)^2+\left(\frac{Re_{ax}}{a_4}\right)^4\right)$ | | | | | | | | | | | (6) |
| $a_0$ | 177,644 | 31,073.6 | 12,510.4 | 6,996.58 | 4,649.33 | 3,428.73 | 2,708.02 | 2,509.08 | 2,452.51 | 2,243.59 | 1924.69 | 1746 |
| $a_2$ | 43.81 | 40.2 | 38.42 | 37.43 | 36.82 | 36.45 | 36.22 | 36.16 | 36.14 | 36.08 | 36.00 | 35.97 |
| $a_4$ | 103.9 | 74.23 | 69.26 | 67.23 | 66.24 | 65.71 | 65.45 | 65.39 | 65.37 | 65.33 | 65.31 | 65.34 |

**TABLE 3** Experimentally derived critical Taylor numbers

| $\Lambda$ | $Ta_{c1}$ Taylor vortex flow | $Ta_{c2}$ wavy vortex flow | $Ta_{c3}$ modulated wavy vortex flow | Reference |
|---|---|---|---|---|
| 0.883 | 120 | 185 | 982 | 14[a] |
| 0.877 | 120 | 151 | Not available | 31 |
| 0.85 | 125 | 165 | 680 | 33 |
| 0.687 | 79 | 387 | 1793 | 33 |

[a]Values derived from a digitized figure.

15475905, 2021, 5, Downloaded from https://aiche.onlinelibrary.wiley.com/doi/10.1002/aic.17228, Wiley Online Library on [09/07/2024]. See the Terms and Conditions (https://onlinelibrary.wiley.com/terms-and-conditions) on Wiley Online Library for rules of use; OA articles are governed by the applicable Creative Commons License

instabilities are absent.[50] The group further showed that shear-thinning causes an increase in the mixing time of the vortices because of a lessened circulation as well as higher axial dispersion of fluid in the TCR.[52]

While the aforementioned flow patterns are the most common ones, a few additional flow regimes can be observed as explained in the following, namely: cavitating Taylor-Couette, global heat convection flow, stable vortices, or the alternation of the latter two. It has been shown that the pressure gradient between rotor and shell is large enough to cause cavitation, given the use of a fluid with a sufficiently low vapor pressure.[36] For this to occur, the transition to the Taylor-Couette flow and the undercutting of the vapor pressure have to be reached simultaneously. This flow regime is termed as the cavitating Taylor-Couette flow. The critical Taylor number is unchanged by the presence of the vapor. Further, a nonuniform temperature field along the TCR influences the flow dynamics. If an axial temperature gradient exists along the TCR, three additional sub flow patterns can be classified for the Taylor Couette flow.[53] These depend on the ratio of centrifugal and buoyancy forces. When the latter are dominant, global heat convection is observed without Taylor vortices even above the critical Taylor number. If centrifugal forces are sufficiently high to suppress buoyancy, stable vortices generate. If both forces are equally dominant, Taylor vortices and global heat convection appear alternately. In the latter case, while the vortices collapse, the mixing is significantly promoted by the heat convection, leading to an irregular transport.

For a system with counter-rotating cylinders, complexity increases significantly as it results in a large variety of different sub-flow regimes depending on the inner and outer Taylor number $Ta_o$ and $Ta_i$.[14] However, to our knowledge no application regarding chemical or biochemical conversions has been developed as yet.

## 3 | ENGINEERING ASPECTS AND GEOMETRIC DESCRIPTORS

With the fundamentals of the Taylor-Couette flow presented in Chapter 2, this chapter focusses on the engineering aspects of the TCR including advances in design, residence time distribution, mass transfer and multiphase mixing, and heat transfer.

The standard TCR consists of a cylindrical shell where an inner cylinder is inserted to form an annular gap. While either the cylinder can be rotated with the angular velocity $\omega$ or cylinder and shell can be counter- or co-rotated, in most applications in process technology, the shell is fixed.[35] Figure 4 defines the design parameters: diameter of the inner cylinder $d_i$, inner ($d_o$) and outer diameter ($D$) of the shell, and reactor height ($H$).

While the dimensions of the reactor can vary significantly, some design rules can be extracted from literature. Commonly, the cylindrical system is defined by two ratios: the aspect ratio $\Gamma$, in Equation (6), and the diameter ratio $\Lambda$, in Equation (7).[14] These two ratios allow for

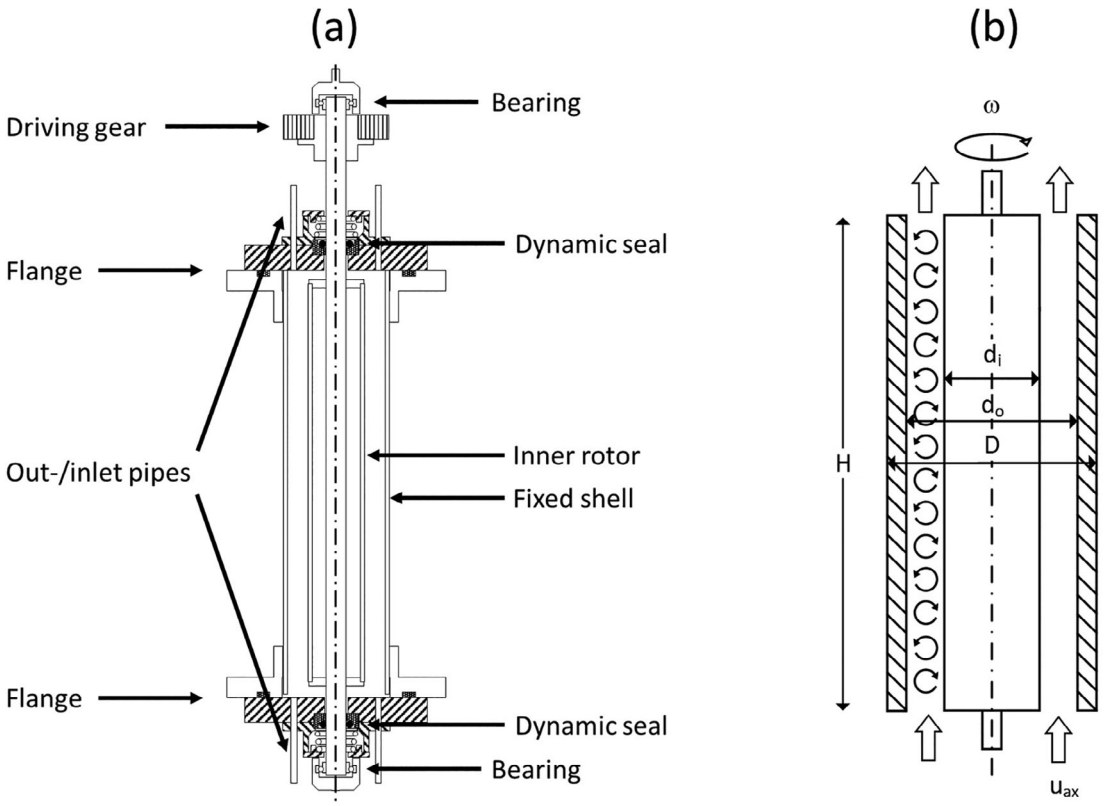


**FIGURE 4** Technical drawing (a) showing a typical TCR setup and schematic depiction (b) defining the design parameters. Technical drawing redrawn based on Kataoka et al.[79]

15475905, 2021, 5, Downloaded from https://aiche.onlinelibrary.wiley.com/doi/10.1002/aic.17228, Wiley Online Library on [09/07/2024]. See the Terms and Conditions (https://onlinelibrary.wiley.com/terms-and-conditions) on Wiley Online Library for rules of use; OA articles are governed by the applicable Creative Commons License

simple design and scaling of TCRs. Another important dimension is the gap width $d$ (Equation (8)). Snyder postulated that the end effects of the cylinder openings are negligible at $\Gamma > 10$,[54] but also higher aspect ratios of up to 480 were used.[32] The diameter ratio on the other hand was initially proposed to allow the formation of stable toroidal vortices above the diameter ratio of $\Lambda = 0.75$,[55,56] and shortly afterwards it was shown that diameter ratios down to $\Lambda = 0.65$ are also feasible.[57] As of now, the lowest reported diameter ratio for Taylor-Couette flow goes down to $\Lambda = 0.5$.[58,59] Still, the Taylor-Couette flow is a gap phenomenon,[41,60] significantly reducing the reactor volume in relation to the volume of the apparatus.

$$\Gamma = \frac{H}{d} \tag{6}$$

$$\Lambda = \frac{d_i}{d_o} \tag{7}$$

$$d = (d_o - d_i)/2 \tag{8}$$

In the traditional design, the injection of fluids is limited to the upper and lower end of the apparatus, limiting the amount of fluid that can be injected without deteriorating the vortex structure.[61] Therefore, Wilkinson and Dutcher introduced a rotor design that enables a radial fluid injection even with both the shell and cylinder rotating.[62] The design is illustrated in Figure 5. They were able to inject liquid and gas along 16 injection points without changing the corresponding critical numbers for flow instabilities. While the highest mass flow studied did modify the Taylor vortex structure when injected for a sustained period, the enlarged vortices returned to the preinjection structure at lowered injection rates. To further study the stability of vortices to injection, the authors introduced a dimensionless stability number given in Equation (9) that relates the injection time $t_{inj}$ and average linear velocity $u_{inj}$ to the effective dispersion coefficient $D_{z,eff}$.[61] This allows estimating the maximum injection speed for a given $Ta$ and injection mass. When the time scale of injection is shorter than the required time for the mass to be transported through the vortex (high stability numbers), the flow conditions become unstable. With $\Lambda$=0.65 and $\Gamma$=60, the authors found that for their tested conditions the vortices became unstable at a stability number above 430,000.

$$\text{Stability number} = \frac{t_{inj} u_{inj}^2}{D_{eff}} \tag{9}$$

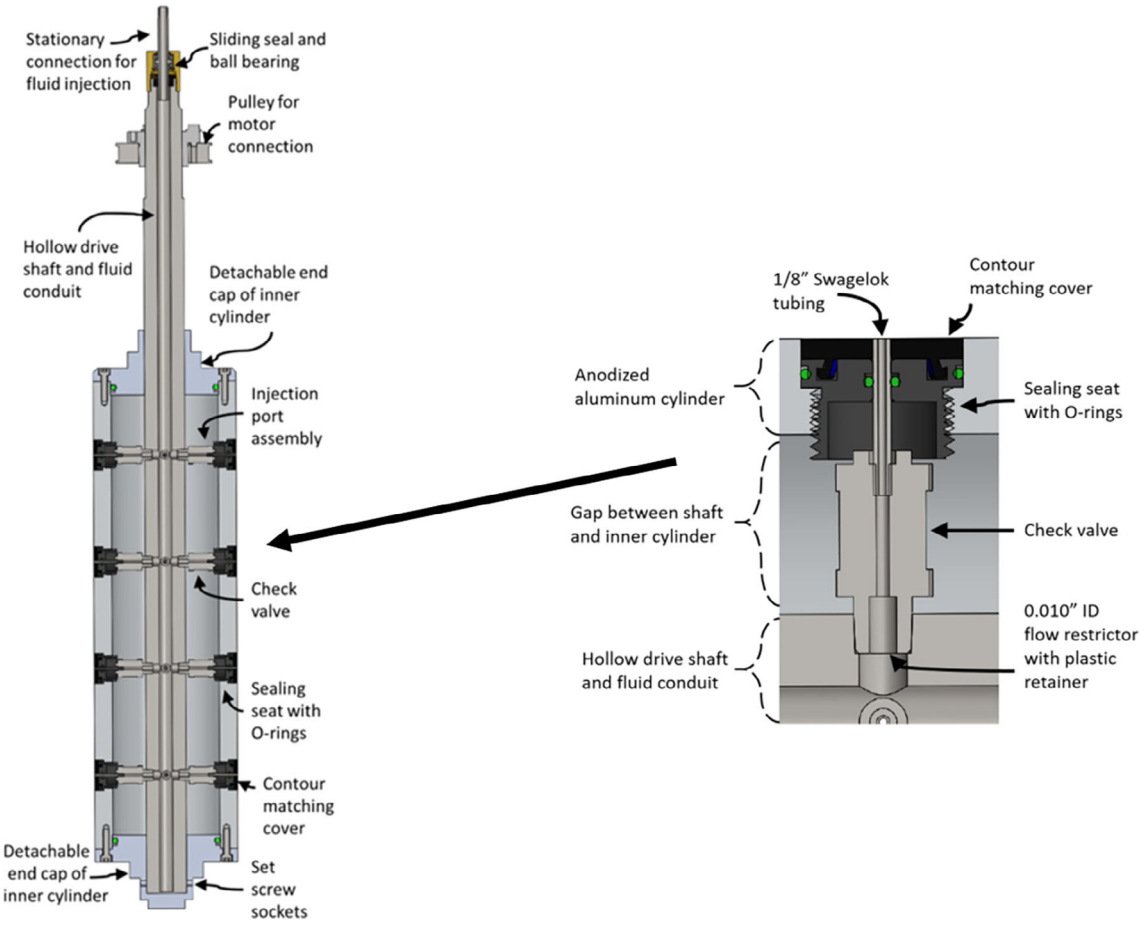


**FIGURE 5** TCR with radial fluid injection ports as shown by Wilkinson and Dutcher.[62] Reproduced with permission from Cambridge University Press. Copyright 2018 [Color figure can be viewed at wileyonlinelibrary.com]

15475905, 2021, 5, Downloaded from https://aiche.onlinelibrary.wiley.com/doi/10.1002/aic.17228, Wiley Online Library on [09/07/2024]. See the Terms and Conditions (https://onlinelibrary.wiley.com/terms-and-conditions) on Wiley Online Library for rules of use; OA articles are governed by the applicable Creative Commons License

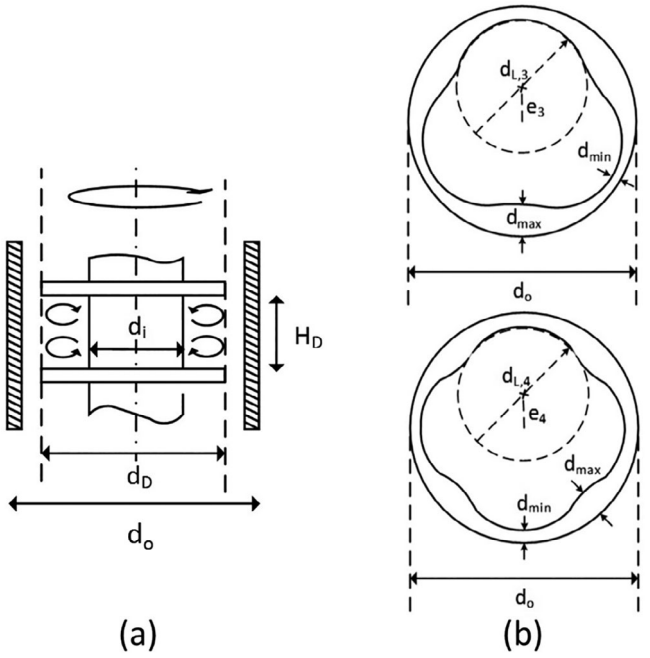


**FIGURE 6** (a) Side-view of Ribbed and (b) cross-section of lobed rotor design with dimensions (drawn based on References 35, 63, 64)

The geometry of the rotor influences the flow characteristics like shear rate, residence time distribution (RTD), and the relationship between flow regime and *Ta*. Figure 6 presents two modified rotor geometries. While the standard TCR design comprises even surfaces, also (a) ribbed and (b) lobed modifications of the rotor were studied.[35,63,64] Design (a) results in very narrow RTD of the reactor, shifting it further to ideal plug flow behavior. The ribs immobilize and stabilize the vortices, reducing the axial dispersion while simultaneously increasing the degree of micromixing.[35] This is beneficial for reactions with longer reaction times or low axial flow rates when no back mixing is desired.[35] The lobed inner cylinder (b) on the other hand, strongly influences the distribution of shear forces in the annular gap.[64,65] Soos et al. showed that especially for larger gaps, the lobed version has a lower power input per volume compared with the standard straight model, which is favorable for example, when using full cells that can be destroyed by shear forces.[64,65] This characteristic makes it especially useful if an even distribution of shear forces is wanted. To increase the shear stress instead, Forney et al. proposed the rotor design depicted in Figure 7.[66] This design deliberately creates cavitation at very high rotational speeds to achieve high shear forces. The high degree of shear originating inside the reactor leads to small bubble sizes within the reactor as consequence, which increase mass transfer rates, hence explaining this efficiency. The determination of the shear stress is relevant in a variety of applications, especially in biochemical processes.[46,67,68] Sobolík et al. derived Equation (11) for the mean wall shear rate $\gamma_w$ at the outer cylinder for various aspect ratios $\Lambda$ as a function of the Taylor number $Ta'$, which was defined following Equation (10).[69] The fitting parameters of the equation for different aspect ratios are summarized in Table 4.

$$Ta' = Ta \cdot \sqrt{\frac{2d}{d_i}} \tag{10}$$

$$\frac{\gamma_w}{\omega} = a \cdot Ta'^{-2} + b \cdot Ta'^{c} \tag{11}$$

Two groups independently invented design (a). In 2008, Richter et al. studied the effect of the rotor shape on the mixing characteristics of a TCR.[35] With the aim to find a rotor shape that suppresses extensive back mixing on the macroscale while at the same time allowing high *Ta* required for intensive micromixing the authors found that a ribbed rotor design is suitable. Siebenhofer et al. on the other hand studied the rotating disc contactor and found that its design can be fundamentally simplified and optimized by showing that stator rings are actually not required to stabilize the toroidal flow pattern.[41] Due to the new design being a hybrid between a rotating disc contactor and the TCR, it is termed the Taylor-Couette disc contactor (TCDC). They further showed that the TCDC provides a high hydraulic load, and studied the effect of rotation rate and dispersed phase holdup on the droplet size and residence time distribution.[70] They were further able to predict the minimum rotation rate necessary for the formation of fully developed toroidal vortices in a single compartment for given operating conditions. From these studies, the investigated optimal design recommendations for the TCDC ended up in Equations (12) to (14).[41,60]

$$d_D = (0.85...0.9) \cdot d_o \tag{12}$$

$$d_i \approx 0.5 \cdot d_o \tag{13}$$

$$H_D = (0.65...1) \cdot (d_o - d_i) \tag{14}$$

A cross-sectional drawing of a lobed rotor design can be seen in Figure 6 (b). Soos et al. found that in comparison to standard TCRs the lobed cylinders have a narrower RTD, with more radii leading to a more slender RTD.[64] The authors recommend the design rules given in Equations (15) and (16) for a design with three, and the design ratios given in Equations (17) to (19) for a design with four radii.

$$d_{L,3} = d_0 - d_{max} + 2d_{min} \tag{15}$$

$$e_3 = d_0 - \frac{d_{max}}{2} + d_L \tag{16}$$

$$d_{L,4} = \left[a - b \cdot \cos\left(\frac{\pi}{4}\right)\right] \cdot \left[1 - \cos\left(\frac{\pi}{4}\right)\right]^{-1} \tag{17}$$

$$a = \frac{d_0}{2} - d_{max}\, b = \frac{d_0}{2} - d_{min} \tag{18}$$

$$e_4 = \frac{d_0}{2} - d_{min} - \frac{d_{L,4}}{2} \tag{19}$$

Other than modifications of the rotor design, the addition of solid particles can further intensify mixing in a TCR. Charton et al. studied the

15475905, 2021, 5, Downloaded from https://aiche.onlinelibrary.wiley.com/doi/10.1002/aic.17228, Wiley Online Library on [09/07/2024]. See the Terms and Conditions (https://onlinelibrary.wiley.com/terms-and-conditions) on Wiley Online Library for rules of use; OA articles are governed by the applicable Creative Commons License

enhancement of mixing in a TCR adding solid spherical particles and found the existence of significant particle-induced mixing in Taylor-Couette flows.[71] The authors concluded that the particles modify the hydrodynamic parameters such as regime stability and axial wavelength in addition to mixing enhancement by inter-particle interactions. The authors further argue that the particles interact with the less mixed outer layers of the vortices which in their system ($d_i$ = 24 mm, $\Gamma$ = 58, $\Lambda$ = 0.687) was experimentally estimated to be 850 μm in thickness. Of the three tested particle sizes of 800, 1,000, and 1,500 μm, only with the latter two, that where larger than the aforementioned layer, an enhancement was observed. Similar results were obtained by Charton et al. for neutrally buoyant particles that significantly enhanced the mixing of a passive tracer injected into the gap.[72] The enhancement increased with increasing particle size and concentration. The authors argue that while particles cross the fluid streamlines, fluid is dragged along, which modifies the spatial gradients. Particles that are trapped close to stagnation points or that stand between vortices enhance the inter-vortex dye migration. This shows how the addition of solid particles is beneficial for the mixing performance of the TCR, of relevance for applications with solid catalyst particles.

## 3.1 | Residence time distribution

The RTD of a reactor is an important aspect of reactor design. As discussed, the TCR exhibits a RTD that approaches that of a cascade of stirred tanks with each vortex being fully back-mixed. This can be favorable for instance in a reactive system whose kinetics display a high order in substrate concentration but is not affected by side or consecutive reactions.[73,74]

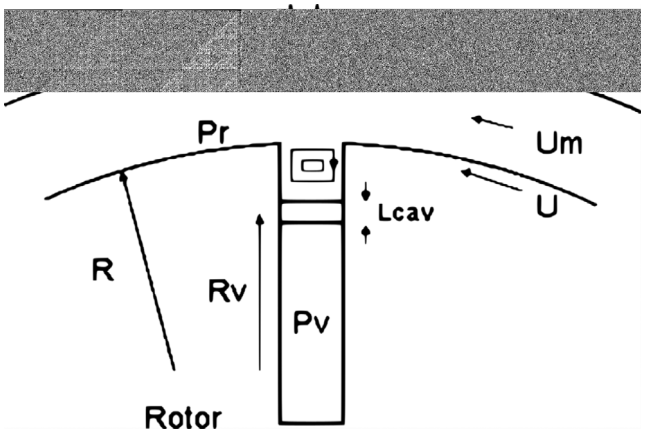


To evaluate the RTD of a reactor setup, the Péclet number *Pe* is of interest. For mass transfer it is defined as shown in Equation (20) for the specific length *b*. It represents the ratio of advective mass transport to diffusive mass transport. For an ideal continuous stirred tank reactor (CSTR), *Pe* becomes 0 while an ideal plug flow reactor (PFR) corresponds to an infinite *Pe* [75]. In Equation (20), $D_z$ is a quasi intervortex diffusion coefficient describing the transfer of components from one vortex to the next. For the TCR, the reactor length or height *H* is usually used as the characteristic length.

$$\mathrm{Pe} = \frac{H \cdot u_{ax}}{D_z} \tag{20}$$

With each individual vortex resembling a CSTR with only limited intermixing, the RTD of the TCR can be approximated by a series of stirred tanks, with *Pe* being between that of an ideal CSTR and an ideal PFR.

As the RTD of a TCR mainly depends on the mass transfer between the vortices, the TCR allows for an adjustable amount of back mixing depending on the applied flow conditions presented by *Ta* and $Re_{ax}$, and the geometry of the reactor. This is also evident in the correlations for *Pe* presented below. Giordano et al. investigated water and water glycerol mixtures in a TCR ($\Lambda$ = 0.48, $\Gamma$ = 11.19) with low axial velocity $Re_{ax}$ = 1–1.5 for 2,410 < *Ta* < 11,793.[76] For this range, *Pe* was described by Equation (21). Moore et al. implemented the axial flow condition into the correlation shown in Equation (22) varying $0.731 < \Lambda < 0.957$, $22 < \Gamma < 161$, $0.5 < Re_{ax} < 30$, and $150 < Ta < 16{,}930$.[21] Tamhane et al. derived two equations for systems without (Equation (23)) and with helicoidal baffles (Equation (24)) for defining *Pe* as a function of reactor design parameters ($\Lambda$ = 0.833, $\Gamma$ = unspecified) as well as fluid characteristics for *Ta* ranging between 7,832 < *Ta* < 23,545 ($d_i$ = 50 mm), 70,668 < *Ta* < 211,849 ($d_i$ = 150 mm), and 196,214 < *Ta* < 588,642 ($d_i$ = 250 mm), where *p* is the pitch of helical baffles that reduced the axial mixing.[77]

$$\mathrm{Pe} = 0.38 - 2.85 \cdot 10^{-5} Ta \tag{21}$$

$$\mathrm{Pe}^{-1} = 7.2 \cdot 10^{-3} \left(\frac{2d}{d_i}\right)^{-0.28} \cdot Ta^{1.05} \cdot (2Re_{ax})^{-0.83} \cdot \left(\frac{2d}{H}\right) \tag{22}$$

$$\mathrm{Pe} = 16.03 \left(\frac{\omega \cdot d_i^2 \cdot \rho}{2\pi \cdot \eta}\right)^{-0.71} \left(\frac{u_{ax} \cdot d_i \cdot \rho}{\eta}\right)^{0.82} \tag{23}$$

15475905, 2021, 5, Downloaded from https://aiche.onlinelibrary.wiley.com/doi/10.1002/aic.17228, Wiley Online Library on [09/07/2024]. See the Terms and Conditions (https://onlinelibrary.wiley.com/terms-and-conditions) on Wiley Online Library for rules of use; OA articles are governed by the applicable Creative Commons License

$$\mathrm{Pe} = 139.53\left(\frac{\omega \cdot d_i^2 \cdot \rho}{2\pi \cdot \eta}\right)^{-0.23}\left(\frac{u_{ax} \cdot d_i \cdot \rho}{\eta}\right)^{0.098}\left(1+\frac{p}{d}\right) \quad (24)$$

Instead of using the dimensionless number *Pe*, some studies focus on the axial dispersion coefficient $D_z$ instead which is related to *Pe* as per its definition in Equation (20). Charton et al. studied the mixing and axial dispersion of Taylor Couette flow patterns during the transition of the Taylor vortex flow toward the wavy vortex flow experimentally and numerically.[32] The authors used two differently sized TCRs. The smaller TCR ($d_i$ = 8.5 mm, $\Lambda$ = 0.85, $\Gamma$ = 480) was used for the range of 107 < *Ta* < 2,136, and the larger TCR ($d_i$ = 24 mm, $\Lambda$ = 0.687, $\Gamma$ = 50) was used for the range of 111 < *Ta* < 27,646. The results indicate that the mixing intensifies with growing *Ta*, causing the mixing within and between adjacent vortices to increase. The authors further showed that for a given *Ta*, the axial dispersion coefficient $D_z$ may vary by a factor of two due to the number of stable wavy states in the wavy flow regime, giving importance to the ramp function for *Ta* used to access the flow pattern. In their study, $D_z$ reached a plateau at higher levels of turbulence. However, Wilkinson and Dutcher argue that the observed plateau stems from the influence of the capillary used to inject the tracer.[61] Using the TCR with radial injection described before, the authors found that $D_z$ smoothly increases with higher level of turbulence instead of reaching a plateau. The correlation given in Equation (25) was derived for the effective dispersion coefficient $D_z$. The authors used a TCR with $\Lambda$ = 0.65 and $\Gamma$ = 60, pressures of up to 4 bar(g), and a *Ta* of up to 10,000, covering all major flow regimes discussed in chapter 2.

$$D_{z,eff} = 1.24 \cdot 10^{-12}\,Ta^2 + 3.11 \cdot 10^{-8}\,Ta + 6.22 \cdot 10^{-6} \quad (25)$$

With the different correlations for *Pe* and $D_z$ shown in this chapter, it is possible to estimate the residence time distribution of a TCR based on the reactor's geometry and the Taylor number. This is especially useful for applications in which the residence time affects the product quality such as it is the case for polymerization reactions. The possibility to include geometric parameters further helps in finding the optimal gap width and reactor height for these applications.

## 3.2 | Mass transfer and multiphase mixing

Understanding the mass transfer characteristics is important in homogeneous systems to study the mixing properties of the setup. In these systems, mixing and axial diffusion of molecules are closely linked to the residence time distribution as discussed in the previous chapter. Thus, this chapter focuses on multiphase systems, where mass transfer is even more relevant considering the existence of phase boundaries and the subsequent mass transfer limitations that may occur. These limitations need to be overcome for an adequate reactor performance.

Diffusion of molecules over a phase boundary can limit reaction or separation rates significantly and is hence a crucial factor in reactor design. Multiphasic mass transfer characteristics are commonly described with the mass transfer coefficient *k*. Because mass transfer resistance from the gas side is oftentimes negligible compared with that of the liquid side, *k* is mostly given for the liquid-side only (hence $k_l$). However, since $k_l$ itself is not easily accessible, in most cases the volumetric mass transfer coefficient $k_la$ as the product of the mass transfer coefficient $k_l$ and the interfacial area *a* is given instead. $k_la$ can be used directly to calculate the flux of components over an interface following the two-film theory by Whitman et al. For this, both the equilibrium concentration and the concentration at the phase boundary must be known.[78]

A common approach to derive design rules to quantify the mass transfer is, as with the other phenomena, to use dimensionless numbers. Here, the Sherwood number *Sh* is used, which can be regarded as the mass transfer analogous to the Nusselt number for heat transfer. Following Equation (26), it is defined as the ratio of the effective mass transfer to the characteristic length *b* to the purely diffusive mass transfer in a static system. It is hence possible to determine $k_l$ using correlations for *Sh* as well as the more accessible diffusion coefficient $D_i$. As in literature different lengths are used for the characteristic lengths, the respective definitions of *Sh* are given in the corresponding equations.

$$\mathrm{Sh} = \frac{k_l \cdot b}{D_i} \quad (26)$$

One of the first studies conducted on TCRs in this field was published by Kataoka et al. in 1977 measuring the flux of ions from electrolytic solutions toward copper electrodes.[79] While no direct correlation was determined, a dynamic investigation of mass transfer was made as a function of the axially moving vortices and the flow determining dimensionless numbers $Re_{ax}$ and *Ta*. The authors found that when no axial flow was introduced, *Sh* showed a significant periodicity in axial direction. This sinusoidal variation of *Sh* is then distorted and its mean value reduced with the addition of axial flow. Thus, it was found that *Sh* increases with increasing *Ta*, but decreases with increasing $Re_{ax}$.

Srinivasan et al. provided correlations for *Sh* for liquid–solid systems using computational methods to solve the differential equations of momentum and continuity for a 2D orthogonal 9,600 cell grid.[80] The authors deduced the equations shown in (27) and (28) for laminar Couette flow and Taylor-vortex flow respectively introducing the Schmidt number *Sc*, which is the ratio of diffusive momentum transfer to diffusive mass transfer (Equation (29)). The correlation parameters are said to be valid for the ranges of $0.3 \leq \Lambda \leq 0.7$, $1 < Ta < 1000$, and $1 \leq Sc \leq 50000$.

$$\mathrm{Sh} = \frac{\mathrm{k_l(2d)}}{D_i} = \frac{12}{\ln\left(\frac{1}{\Lambda}\right)} \cdot \frac{d}{d_i} + 0.0096\,Ta \cdot Sc^{\frac{1}{3}} \cdot \Lambda^{-1.25} \quad (27)$$

$$\mathrm{Sh} = \frac{\mathrm{k_l(2d)}}{D_i} = \frac{12}{\ln\left(\frac{1}{\Lambda}\right)} \cdot \frac{d}{d_i} + \sqrt{0.4232\,Ta} \cdot Sc^{\frac{1}{3}} \cdot \Lambda^{-0.1} \quad (28)$$

$$Sc = \frac{\nu}{D_i} \quad (29)$$

15475905, 2021, 5, Downloaded from https://aiche.onlinelibrary.wiley.com/doi/10.1002/aic.17228, Wiley Online Library on [09/07/2024]. See the Terms and Conditions (https://onlinelibrary.wiley.com/terms-and-conditions) on Wiley Online Library for rules of use; OA articles are governed by the applicable Creative Commons License

Qiao et al. experimentally and numerically studied the oxygen transport in a Taylor Couette bioreactor and derived the correlation in Equation (30).[81] The authors found that the axial position of a single air bubble has an influence on the mass transfer due to higher oxygen concentrations at the top surface of the reactor. If the air bubble was trapped in the vortex center or the rotor wall, the total mass transfer coefficient increased significantly. In the study, the influence of the viscosity on the mass transfer was considered by the addition of glycerol with $\Lambda = 0.67$ and $\Gamma = 9$.

$$\mathrm{Sh} = \frac{k_l d}{D_i} = 0.065\mathrm{Ta}^{0.94}\mathrm{Sc}^{-0.99} \tag{30}$$

Similarly, Chouippe et al. numerically studied the bubble dispersion in turbulent Taylor-Couette flow and found that the rotation of the inner cylinder draws the bubbles toward the inner cylinder due to inertia effects.[58] The outflow jet of the Taylor vortices enhance the global dispersion in the bulk in the radial direction, while the circulation of said vortices generates an accumulation of the bubbles in the outflow regions near the inner cylinder. The authors further found that for large gaps of $\Lambda = 0.5$, the attraction toward the rotor is dominant. Together with the previously presented finding that bubbles close to the rotor wall show a significantly increased mass transfer, it can be concluded that large gaps are beneficial for gas–liquid mass transfer.

Further correlations were later published for *Sh* and $k_l a$ for the absorption of oxygen in water by the group of Vigil et al., as shown in Equations (31) to (35),[82,83] wherein *a* denotes the volumetric interfacial area and $d_{32}$ the Sauter mean diameter of the bubbles. The used TCR had a $\Lambda$ of 0.75, a $\Gamma$ of 40, and $Ta < 3{,}500$. The group further studied the influence of the interfacial tension on the mass transfer by adding ethyl alcohol.[84] Herein, the Morton number *Mo* describes disperse two-phase flows (relation of viscous forces to surface tension). The interfacial tension was varied between 40.6 and 72.5 mPa s, which corresponded to $2.2 \times 10^{-11} \leq Mo \leq 1.2 \times 10^{-9}$.

$$\mathrm{Sh} = \frac{\mathrm{k_l a} d_{32}^2}{D_i} = 1.45 \cdot 10^{-7} \cdot (2Re_{ax})^{0.82} \cdot \left(Ta + 1.47 \cdot 10^4\right)^{1.61} \tag{31}$$

$$\frac{d_{32}}{d} = 1.0 \cdot 10^{-5} (2Re_{ax})^{0.11} \left(Ta + 3.3 \cdot 10^4\right)^{0.91} \tag{32}$$

$$k_l \mathrm{a} = 0.423 \cdot u_{ax}^{0.668} \cdot \left(\frac{\omega}{2\pi}\right)^{0.178} \tag{33}$$

$$\frac{d_{32}}{d} = 1.25 \cdot 10^{-11} (2Re_{ax})^{0.242} \left(Ta + 7.65 \cdot 10^5\right)^{1.676} Mo^{-0.011} \tag{34}$$

$$\mathrm{Sh} = \frac{\mathrm{k_l a} d_{32}^2}{D_i} = 1.15 \cdot 10^{-3} \cdot (2Re_{ax})^{1.057} \cdot \left(Ta + 1.09 \cdot 10^4\right)^{0.914} \cdot Mo^{0.108} \tag{35}$$

As evident in the equations above, for the estimation of the mass transfer in multiphasic systems, the interfacial area is also of interest. The ability of a reactor setup to bring two or more phases in intense contact is determined by a variety of parameters, the most important being the specific power input per volume $PV^{-1}$, the shear stress $\gamma_\Theta$ in the gap, the dispersed phase hold-up $\varphi_d$, and the Sauter mean diameter $d_{32}$ of the dispersed particles. While the former two variables represent the mechanical power transferred into the reaction mixture and the resulting shear stress, the latter two concern the phase dispersion. $\varphi_d$ represents the fraction of a certain phase dispersed (d) by the shear stress into another continuous (c) phase. $d_{32}$ is defined as the theoretical diameter of a particle if the total volume of all particles became equally distributed (bubbles, droplets or solid particles) while maintaining the overall surface area of the initial particle swarm. Hence, Equation (36) relates both parameters to the interfacial area (a) as discussed previously.

$$\mathrm{a} = \frac{6 \cdot \varphi_d}{d_{32}} \tag{36}$$

The dispersion defining characteristics have been addressed recently by a number of groups leading to Equations (32), (34), (37), and (38) for the determination of $d_{32}$ for various conditions.[83-86] For this purpose, different biphasic systems were investigated. As stated before, Vigil et al. investigated a liquid–gas system consisting of water and air without (Equation (32)) and with (Equation (34)) variation of the interfacial tension. Grafschafter and Siebenhofer (TCDC, $d_i = 50$ mm, $d_D = 85$ mm, $\Lambda = 0.5$, $\Gamma = 40$) used the liquid–liquid system ShellSolT-water to derive Equation (37),[86] and Farzad et al. ($d_i = 112.5$ mm, $\Lambda = 0.9375$, $\Gamma$ = unspecified) applied different oil–water liquid–liquid systems to derive Equation (38).[85] The Sauter mean diameter in these correlations is a function of the fluid data and the dimensionless Weber (*We*), Froude (*Fr*) and *Mo* numbers. *We* is an important indicator in the creation of dispersions bringing the destabilizing inertia forces in relation to the stabilizing surface forces in a droplet resulting in small droplets at high *We*. *Fr* on the other hand is the ratio of inertia to gravity in a liquid.[83-86] Siebenhofer et al. further provided a correlation for the dispersed phase hold-up in an oil–water system as shown in Equation (39).[86] It is a function of operating conditions like the rotational speed and the velocity of the dispersed and continuous phase as well as substance properties and dimensionless numbers. The parameters $C_1$ to $C_6$ are available for two different columns of 0.1 m and 0.3 m in diameter and varying hydraulic load.[70,86] It has to be noted that the Equations (37) and (39) are based on correlations for the rotating disc contactor modified for the application on the TCDC and not the TCR.

$$\frac{d_{32}}{d_D} = \mathrm{C_3} \cdot \mathrm{C_4} \cdot \left(\frac{\sigma}{\rho_c \omega^2 d_D^3}\right)^{C_1} \cdot \left(\frac{1}{Fr} \cdot \frac{\Delta\rho}{\rho_c}\right)^{C_2} \tag{37}$$

$$\frac{d_{32}}{d} = We^{-0.0045} \cdot Ta^{-0.4509} \cdot \left(\frac{\mu_d}{\mu_c}\right)^{0.3217} \cdot \left(\frac{\rho_d}{\rho_c}\right)^{-6.2485} \tag{38}$$

$$\varphi = \mathrm{C_3}\left[C_5 + C_6 \left(\frac{u_c + u_d}{d_D \cdot \omega}\right)^3\right] \left(\frac{\sigma}{\rho_c \omega^2 d_D^3}\right)^{0.673} \cdot \left(\frac{1}{Fr} \cdot \frac{\Delta\rho}{\rho_c}\right)^{-2.177} \tag{39}$$

15475905, 2021, 5, Downloaded from https://aiche.onlinelibrary.wiley.com/doi/10.1002/aic.17228, Wiley Online Library on [09/07/2024]. See the Terms and Conditions (https://onlinelibrary.wiley.com/terms-and-conditions) on Wiley Online Library for rules of use; OA articles are governed by the applicable Creative Commons License

The specific power input for the TCR can be calculated following Equation (40) as a function of the torque *M*, the rotational velocity, and reactor design aspects. While this is relatively simple in a setup with two straight cylinders, it becomes increasingly complex for more advanced reactor designs. Soos et al. used two correlations to calculate the *G* for the specific length *b* (Equation (41)) available from Lathrop et al., as shown in Equation (42) to numerically determine the power input of a lobed TCR.[64,67]

$$\mathrm{PV}^{-1} = \frac{8 \cdot \omega \cdot \mathrm{M}}{\left(d_o^2 - d_i^2\right) \cdot H} \tag{40}$$

$$\mathrm{G} = \frac{M}{\rho \cdot \nu^2 \cdot b} \tag{41}$$

$$\mathrm{G} = \begin{cases} 1.45 \dfrac{\Lambda^{1.5}}{(1-\Lambda)^{1.75}} Ta^{1.5} \mid 4 \cdot 10^2 < Ta < 10^4 \\ 0.23 \dfrac{\Lambda^{1.5}}{(1-\Lambda)^{1.75}} Ta^{1.7} \mid 10^4 < Ta < 10^5 \end{cases} \tag{42}$$

The design rules given for the mass transfer are especially useful for multiphase reaction systems and also extend to non-reactive systems such as extractions or absorptions. It is possible to estimate interfacial areas and energy dissipation rates. The Sherwood number can be used to determine the mass transfer performance of the TCR.

## 3.3 | Heat transfer

Heat transfer is required to provide or withdraw energy based on the reactive system and to avoid the formation of hot spots that can be detrimental to selectivity or activity of catalysts. Heat transfer is often characterized by the dimensionless Nusselt number, *Nu*. *Nu* is defined as the ratio between the convective heat transfer of a wall with the length $b = d_o\text{-}d_i = 2d$ to a fluid flowing alongside that wall and the purely conductive heat transfer that would occur in a stationary liquid. Following Equation (43), it is a function of the heat transfer coefficient $\alpha$ from wall to fluid and the thermal conductivity $\lambda_l$ of the fluid itself.

$$Nu = \frac{\alpha \cdot 2d}{\lambda_l} \tag{43}$$

The first studies were conducted in a system with no axial flow ($Re_{ax} = 0$). Ho et al. found that the Nusselt number for pure conduction $Nu_K$ can be described by Equation (44) as a function of the reactor diameters.[87] For a reactor with the gap width $d << d_i$, the equation can be simplified to $Nu_K = 2$.

$$Nu_K = \frac{2\left(\frac{1-\Lambda}{\Lambda}\right)}{\ln\left(\frac{1-\Lambda}{\Lambda} + 1\right)} \tag{44}$$

Based on this equation, the actual *Nu* is then calculated for a TCR with a narrow gap using a power law following expression (45). $Z_1$ is an abbreviation for the empirical term shown in Equation (46). *Nu* therein is a function of the Prandtl number *Pr* (ratio of kinematic viscosity) to thermal conductivity (Equation (47)) and the Grashof number *Gr* (ratio of static buoyancy) to viscous forces (Equation (48)).[87,88]

$$\left(\frac{Nu}{Nu_K}\right)\left(\frac{\tilde{Ta}}{Ta_{c1}}\right)^m = > \left(\frac{Nu}{Nu_K}\right) = \left(\frac{0.5 \cdot Ta \cdot \left(\frac{2d}{d_i}\right)^{0.5}}{0.5 \cdot \pi^2 \cdot \left(1 - \left(\frac{d}{d_i}\right)\right)^{-1} \cdot {Z_1}^{-0.5}}\right)^{\left(\frac{Pr}{Gr}\right)^{1/6}} \tag{45}$$

$$Z_1 = 0.0571\left(1 - 0.652\left(\frac{\frac{2d}{d_i}}{1 - \frac{d}{d_i}}\right)\right) + 0.00056\left(1 - 0.652\left(\frac{\frac{2d}{d_i}}{1 - \frac{d}{d_i}}\right)\right)^{-1} \tag{46}$$

$$Pr = \frac{\nu}{\lambda} \tag{47}$$

$$Gr = \frac{g\beta\Delta T d^3}{\nu^2} \tag{48}$$

Aoki et al. later theoretically derived the equation given in (49).[89] The authors stated that the equation is valid in the range of $Ta_{c1} \leq Ta \leq \min\left(\frac{Ta_{c1}}{\sqrt{1 - 0.535/Pr^2}}, \sqrt{2.2}\, Ta_{c1}\right)$.

$$Nu = 2 \cdot \frac{1-\Lambda}{\Lambda \cdot \ln\left(\frac{1}{\Lambda}\right)}\left(1 + 1.438\left(1 - \left(\frac{Ta_{c,1}}{Ta}\right)^2\right) \cdot \mathrm{Pr}^2\right) \tag{49}$$

Following this, systems with axial flow were further investigated.[79,90,91] However, in the ranges of $Re_{ax}$ = 0–260 and *Ta* = 35–9,200, due to neglecting the $u_{ax}$, the error of the estimations was found to be 30%–50% when applied to a system with axial flow.[79]

Later, a mathematic expression was derived by Simmers et al. for the temperature drop over the gap ($\Delta T$, Equation (50)) and *Nu* as a function of *Pr*, $Re_{ax}$, *Ta* as well as design parameters of the TCR (Equation (51)–(53)).[91] The temperature drop measured in the TCR ($d_i$ = 111.8 mm, $\Lambda$ = 0.8 and 0.955, $\Gamma$ = 130) was described depending on the fluid density $\rho$, the specific heat capacity $c_p$, the shear stress at the wall at Taylor-Couette vortex flow $\gamma_w$, and the radii design ratio $\Lambda$. The flow conditions were set to $150 < Re_{ax} < 800$, and $Ta_{c1} < Ta < 2{,}000{,}000$.

$$\Delta T = \frac{\dot{q}}{\rho \cdot c_p}\left(\frac{\rho}{\gamma_w}\right)^{0.5} \cdot 0.5\left(\frac{\Lambda \cdot \mathrm{Ta}_{c,1}^2 \cdot \frac{d}{r_i}}{1-\Lambda}\right)^{0.25} \cdot \left(Pr + \ln\left(1 + Pr \cdot \exp\left(\left(\frac{1-\Lambda}{\Lambda \cdot Ta_{c,1}^2 \cdot \frac{d}{r_i}}\right)^{0.25} \cdot \frac{2}{3}\left(\frac{\rho \cdot \omega^2}{\gamma_w}\right)^{0.5} - 1\right) - \mathrm{Pr}\right)\right) \tag{50}$$

$$Nu = \frac{4Pr \cdot (2Re_{ax})^{0.5} \cdot \left(Ta^2 \cdot \frac{d}{r_i}\right)^{0.3675}}{Z_2\left(\frac{Z_3}{1-\Lambda}\right)^{0.5}\left(\frac{\Lambda}{1-\Lambda}\right)^{0.25} \cdot \left(Ta_{c,1}^2 \cdot \frac{d}{r_i}\right)^{0.61275}} \tag{51}$$

15475905, 2021, 5, Downloaded from https://aiche.onlinelibrary.wiley.com/doi/10.1002/aic.17228, Wiley Online Library on [09/07/2024]. See the Terms and Conditions (https://onlinelibrary.wiley.com/terms-and-conditions) on Wiley Online Library for rules of use; OA articles are governed by the applicable Creative Commons License

$$Z_2 = Pr + \ln\left(1 + Pr \cdot \exp\left(\frac{2}{3}\left(\frac{1-\Lambda}{\Lambda}\right)^{0.25}\left(\frac{\Lambda \cdot Z_3}{(1-\Lambda)^2}\right)^{0.5}(2Re_{ax})^{-0.5} \cdot \left(Ta^2\frac{d}{r_i}\right)^{0.1325} \cdot \left(Ta_{c,1}^2\frac{d}{r_i}\right)^{0.1175} - 1\right) - Pr\right) \quad (52)$$

$$Z_3 = \frac{\left(1 + \Lambda^2 + \frac{1-\Lambda^2}{\ln(\Lambda)}\right)}{2 + \frac{1-\Lambda^2}{\ln(\Lambda)}} \quad (53)$$

Torii et al.[92] derived Equation (54) based on the work of Donne and Meerwald[90] for a turbulent system at $\Lambda$ = 0.8, 3,000 < $Re_{ax}$ < 5,000, and $Ta$ = 0 and 10,000. This leads to an expression with no influence of $Ta$.

$$Nu = \left(0.0189 \cdot (2Re_{ax})^{0.8} \cdot Pr^{0.4}\right) \quad (54)$$

Since computational power is more readily available, computational fluid dynamics (CFD) studies allow to obtain more fundamental insights into the heat transfer with one of the earlier studies conducted by Kedia et al.[93-96] Lopez et al. obtained results in a computational heat flow study that revolves around a direct numerical simulation of the Navier–Stokes equation for a Taylor-Couette flow over a wide range of aspect ratios $\Gamma$ and $\Lambda$ as well as Prandtl and Rayleigh numbers (Raleigh number Ra is the relation of convective to conductive heat transfer in a buoyancy-driven flow).[96] For a more exhaustive overview over the advances made to understand the heat transfer in the TCR, it is referred to review of Fénot et al..[97]

## 4 | APPLICATION OF THE TCR IN PROCESS TECHNOLOGY

The specific advantages of the TCR make this reactor concept an interesting alternative to more conventional types. Subsequently, TCRs have been applied in a wide array of topics within process technology. Table 5 presents an overview of the fields where TCRs have been applied that will be expanded in the next sections together with the main advantages associated to their use.

### 4.1 | Homogeneous transition metal catalyzed reactions

One of the main advantages of the TCR relates to its good mixing properties. Especially for homogeneous transition metal catalysis, the advantages lie on the narrow residence time distribution. These reactions generally require longer reaction times that benefit from the low back mixing. The group of Behr investigated the applicability of the TCR in the transformation of renewable resources using transition metal catalysis and thermomorphic solvent systems (TMS) for the recovery of the valuable catalyst.[63,98] In a TMS, a temperature dependent miscibility gap allows easy separation of catalyst and product phase by decantation after the reaction step. After initial investigations, a suitable recycling concept and solvent combination, as well as a suitable catalytic system, the hydroamination of β-myrcene was transferred from the lab to a continuously operated TCR.[99] The TMS consisted of dimethylformamide and n-heptane.[63,98,99] One of the challenging aspects of the hydroamination is the side isomerization/dimerization and the telomerization that have to be suppressed to achieve an efficient production. The continuous miniplant consisted of the reactor, a phase separator unit and the required pump and

**TABLE 5** Summary of the applications and features of Taylor-Couette reactors in process technology

| Application | Main aspects associated with TCR configurations |
|---|---|
| Homogeneously catalyzed reactions | Narrow residence time distribution aids homogeneously catalyzed reactions owing to their commonly longer reaction times that benefit from low back mixing. Adjustable degree of back mixing influences the concentration profile along the reactor axis allowing further optimization. |
| Photocatalysis and light induced applications | High uniformity of mixing in the annular gap leads to well dispersed suspensions of heterogeneous solid catalysts allowing using a single radiation source. Fluid flow capable of rapidly moving solids like microalgae between light and dark regions |
| Enzymatic transformations and biotechnology | Low and uniform shear forces in the liquid phase cause controlled strain on fragile biological components (e.g., immobilized supports or cells). Enhanced heat transfer. |
| Polymer synthesis | High specific surface areas, which enhances heat transfer in highly exothermic reactions like polymerization. Controllable and narrow particle size distribution. In most cases, residence times are significantly reduced with respect to stirred tanks. |
| Crystallization and solid processing | Uniformity in the fluid dynamic conditions offers great advantages for crystallization purposes allowing obtaining narrow crystal/particle size distributions. |
| Aggregation and flocculation of fines | Aggregation of fine particles in suspension can be facilitated by controlled shear stresses generated in Taylor-Couette flow, allowing fine-tuning of floc size in water treatments. |

15475905, 2021, 5, Downloaded from https://aiche.onlinelibrary.wiley.com/doi/10.1002/aic.17228, Wiley Online Library on [09/07/2024]. See the Terms and Conditions (https://onlinelibrary.wiley.com/terms-and-conditions) on Wiley Online Library for rules of use; OA articles are governed by the applicable Creative Commons License

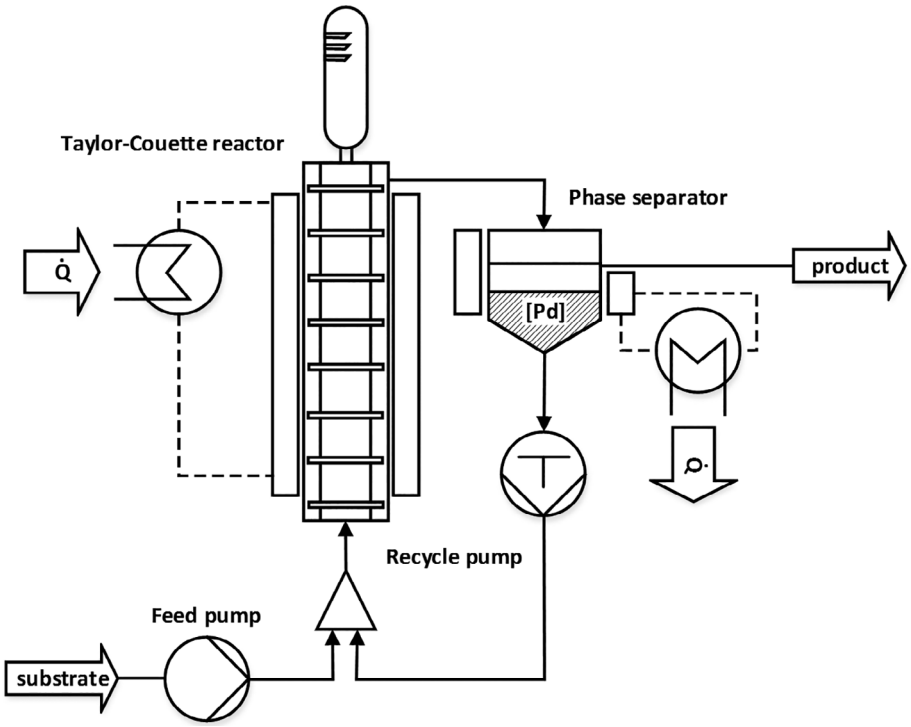


**FIGURE 8** Miniplant featuring a Taylor-Couette reactor for the hydroamination of β-myrcene constructed by Färber and Behr (based on Reference 99)

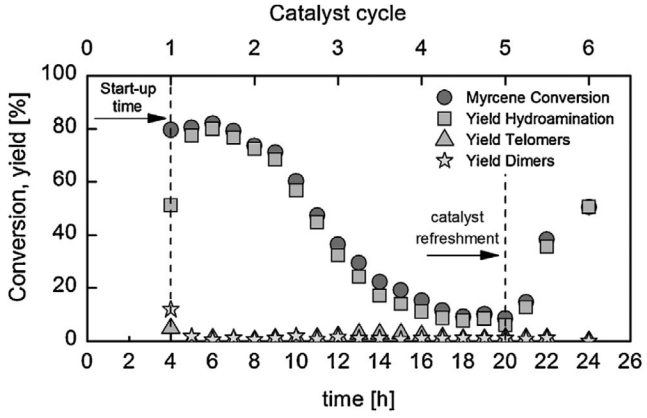


**FIGURE 9** Yield and conversion of the continuous hydroamination of β-myrcene in a dimethyl formamide/n-heptane solvent system as reported by Färber et al.[99] Reprinted from Färber et al. with permission from Elsevier. Copyright 2016

thermostats as shown in Figure 8.[100] As the main outcome of the application of the TCR, it was shown that it is capable of delivering high degrees of segregation, which in turn leads to residence times of several hours. This is a very favorable aspect for cases where the reaction can take several hours to complete. Operating in such a reactor setup, it was possible to generate similar results to previous batch-experiments on a laboratory scale. The time resolved yield of amines and conversion of substrate during the continuous operation is shown in Figure 9, reaching a conversion of myrcene of 82% and a yield to the terpenyl amine of 80%. The catalyst deactivated over the course of the experiment, presumably due to accumulation of the homogeneous palladium catalyst at the heated inner cylinder.[100] In this case, the system could be reactivated through catalyst refreshment and reintroduced in the TCR. In summary, despite TCRs providing a favorable flow capable of ensuring long residence times, fouling could be an issue over long term experiments and should not be ignored.

## 4.2 | Photocatalysis and light induced applications

The application of a TCR in the field of photocatalysis is especially beneficial because of the uniform mixing in the annular gap. This mixing behavior results in a uniform suspension of the heterogeneous particles, making it possible to use a single source of radiation.

Several authors discuss the degradation of organic pollutants and contaminants in a TCR. The degradation of formate was investigated by periodically illuminating the reaction volume from inside the inner cylinder (CPI, "controlled periodic illumination") to improve the light efficiency of the process.[101] In this way, the efficiency of the photoinduced reaction was increased by up to a factor of three. Such efficiency was strongly influenced by the rotation velocity applied to the inner cylinder.

Sengupta et al. investigated the application of two Taylor-Couette reactors of varying geometry in the heterogeneous degradation of organic pollutants (phenol and textile dyes).[102] A heterogeneous $TiO_2$ coating on the rotor was used to catalyze the process under wavy vortex flow. In comparison to a classic plug flow regime for photocatalysis, the efficiency of the reaction was increased between 60% and 125%. The authors attribute this to an enhancement of mass transfer of the pollutants to the catalyst and back, which is significantly improved by the specific flow pattern in the TCR.

15475905, 2021, 5, Downloaded from https://aiche.onlinelibrary.wiley.com/doi/10.1002/aic.17228, Wiley Online Library on [09/07/2024]. See the Terms and Conditions (https://onlinelibrary.wiley.com/terms-and-conditions) on Wiley Online Library for rules of use; OA articles are governed by the applicable Creative Commons License

More work on the photocatalytic degradation of phenol was investigated varying several influencing factors.[103] Apart from proposing a kinetic model for the reaction, the authors also scaled up the TCR increasing the gap width. The delivery of light into the reactor was changed in this study from regular continuous to controlled periodic illumination to investigate the influence on the degradation of the pollutants. Nevertheless, a correlation of the performance of the reaction and the type of illumination was not found.[103] Further investigations focused on the different phases of vortex formation and the influence of the finite reactor length using time dependent calculation methods.[104] The authors discuss maximizing the degradation of pollutants by combining mixing by aeration in the annular gap with periodic illumination.

The group of Forney considered fast photocatalytic reactions, like the oxidation of iodide ($I^-$) to iodate ($I_3^-$).[105] They developed a law of similarity for the product development incorporating Taylor-vortices and investigated the optimal operating parameters of the TCR ($Ta$, $\omega$) to maximize photoefficiency, which occurred when the radiation penetration depth equals the boundary-layer thickness. Furthermore, the authors compared the same chemical reaction in a square tube and a gap between two concentrical cylinders without rotation with the TCR,[106] where the latter outperformed both geometries considerably. This undoubtedly indicates that the mixing induced by Taylor regimes are beneficial in light induced reactions.

Dutta and Ray numerically and experimentally investigated the degradation of organic components like Orange II, Eosin B and benzoic acid, especially focusing on the influence of *Re* and catalyst loading.[107] Different reactor types and the use of suspended catalyst versus immobilized catalyst particles on the rotor surface were compared. For the TCR, in conclusion, the difference between suspended and immobilized particles was insignificant.

Haim and Pismen performed computational simulations for Taylor vortices in a photocatalytic reaction of first order with an illuminated rotor. The authors recommend this flow pattern when compared with laminar flow for fast-occurring reactions with strong attenuations.[108]

The TCR setup has also been proposed as an efficient concept for sterilization purposes via UV irradiation. Recently, a study on the application of UV-C to assess the inactivation kinetics of *Escherichia coli* ATCC® 8739™ was developed. In particular, the performance of a TCR was evaluated and compared with an annular reactor system, which led to the inactivation of *Escherichia coli* being similar between the two when no rotation force was applied. When a coiled tube system was used (whose RTD was narrower), the latter showed better microbial reduction than the aforementioned thin film systems. However, in spite of the laminar flow conditions, the reactor performance of the TCR upon rotation of the inner cylinder is comparable to that of the coiled tube under turbulent flow.[109] Prior to these findings, TCRs had already been used in other continuous disinfection processes using UV radiation.[110,111] Especially the uniform flow in the reactor as well as the good internal mixing are seen as beneficial for inactivation of *E. coli* cells. Forney et al. proposed a modification of the Taylor-Couette reactor by adding a wavy rotor ("rotor wavy wall"), which was found to outperform the classic rotor design under Taylor-Couette flow.[111]

In further investigations, the rotor of the TCR was modified with holes, as depicted in Figure 7, and operated at very high rotational speeds in turbulent regime to deliberately create cavitation.[66] With the UV-induced oxidation of iodide ($I^-$) to iodate ($I_3^-$), the mixing properties under these conditions (high $\omega$) are similar to a CSTR. Furthermore, introducing UV-light, thermal effects and the high shear forces led to an inactivation of up to 99.4% of *E. coli* bacteria in water using this modified design of TCR. The best inactivation rates were achieved operating the reactor in the laminar Taylor-vortex flow regime. To test the relevance of mixing in this setup, the authors added a soluble dye to the medium, which caused the inactivation of *E. coli* to decline ~50% due to photon absorption of the dye in this regime.[66]

Investigating disinfection using UV light, another study focused on the geometric proportions as well as the length and form of the Taylor-Couette photoreactor.[112] A significant difference between narrow and tall or wide and short reactors was not found under the same flow conditions and UV intensities.

Finally, algal biomass growth has also been explored with TC photo-bioreactors. Vigil et al. developed intensive work on Taylor vortex photo-bioreactors for the growth of *Chlorella vulgaris*. This setup has proven to generate fluid flow capable of rapidly moving microalgae between light and dark regions, which lowers the photosynthetic turnover time. Such flow structures result in higher photoefficiency and $CO_2$ uptake rates owing to bubble induced mixing, which in the end lead to higher algal biomass productivity.[113]

In subsequent work, the same authors characterized the reactor by quantifying mixing, mass transfer and algal biomass growth rates within the reactor. Taylor vortices in principle can improve growth rate owing to enhanced light utilization efficiency and also have an influence on mixing and mass transfer at the interphase between the gas bubbles and the liquid. However, by comparing the time scales for these three effects, the algal biomass growth rate was mostly affected by the improvement in light utilization rather than being limited by mass transfer or mixing.[114]

Finally, the same authors present two thorough quantitative computational studies in parallel combining fluid hydrodynamics, simulation of light transport in the reactor and how both affect biomass growth. One of such studies follows a Lagrangian approach,[115] whereby algal growth appears to be overestimated, which may be due to the limitations of the model concerning the availability of nutrients in the media as well as particle tracking. The other reference concerns a CFD model following a Eulerian approach,[116] which correctly predict biomass productivity increases with increased rates of mixing as well as a limit thereto as such a rate turns too high. Nevertheless, the simulation overpredicts algal productivity at high azimuthal *Re*, which could be ascribed to the most radiation being absorbed near the illuminated surface as the biomass loading becomes too high. In both studies, a common conclusion is that models are still limited for the proper prediction of algal growth at highly concentrated suspensions of algae.[115,116]

With the aforementioned examples of the application of TCRs in light induced applications, it appears that the media in the existing

15475905, 2021, 5, Downloaded from https://aiche.onlinelibrary.wiley.com/doi/10.1002/aic.17228, Wiley Online Library on [09/07/2024]. See the Terms and Conditions (https://onlinelibrary.wiley.com/terms-and-conditions) on Wiley Online Library for rules of use; OA articles are governed by the applicable Creative Commons License

flow get an improved exposure to light sources, thus intensifying the performance of the corresponding processes.

### 4.3 | Applications in enzymatic transformations and biotechnology

The application of a Taylor-Couette reactor in enzymatically catalyzed reactions is especially interesting considering the low and uniform shear forces that the generated vortices exert on the liquid phase. The support of immobilized enzymes can be indeed fragile components that require these gentle degrees of strain.

The group of Giordano and his collaborators have investigated thoroughly different applications in enzymatic conversions. The isomerization of fructose to glucose was studied in a TCR with immobilized glucose isomerase from *Streptomyces rubiginosus* (Spezyme IGI ®) and no damage was observed to the heterogeneous particles while enabling efficient mixing. The reactor was modeled using a simplified lumped triparametric approach to describe mass transfer in TC flow. The performance of the reactor was close to that of a plug flow reactor for low rotational speeds, although at higher $\omega$ the by-pass flow and the mixing between vortices decreased the performance and were worse than a stirred tank.[42] Subsequently, the authors applied immobilized enzymes in the protein cleavage of cheese whey in a continuously operated TCR to obtain a uniform molecular weight distribution without damaging the fragile catalyst beads.[117] Another example is the utilization of immobilized Penicillin G acylase is immobilized in bi-dispersed gel matrix particles for the synthesis of β-lactam antibiotics like ampicillin for which, again, the low strain on solid enzyme supports is also required. In this study, a comparison between a fed-batch TCR configuration and a stirred tank was drawn, the former of which showed very uniform mixing behavior without damaging the enzymes compared with what conventional impellers do in a stirred tank.[118]

In the context of process intensification, where operations like chemical reaction and separations can be performed jointly, Ameer et al. reworked the concept of the TCR combining membrane separation to conform a vortex flow plasmapheretic reactor (VFPR). They used this reactor concept in a heparinisation process employing immobilized heparinase I for the purpose, of interest for kidney failure and heart disease therapies. The VFPR reached high heparin conversions in saline and blood media in addition to no blood damage owing to the controlled shear stress.[119]

TCRs have also proven an effective process intensification tool for the enzymatic hydrolysis of starch and its gelatinization with the additional advantage of the starch granules being less damaged than in an extruder. A first study put the emphasis on the influence of the geometry of the reactor and type of flow on the degree of starch gelatinization,[120] whereas a second work reports on the influence of operational variables like rotation frequency, temperature and initial concentration of starch.[121]

In addition to enzymatic catalysis, TCRs have also been employed for the culture and manipulation of cells owing to the controlled shear stress that can be applied and the potential improvement in biomass yield owing to setups which improve aeration.

For instance, Haut et al. investigated an acrylic glass prototype of an existing commercial bioreactor (Synthecon) for mass transport properties and hydrodynamic characteristics via particle image velocimetry (PIV) and CFD studies in the cultivation of living animal (Chinese ovary hamster) cells in suspension. These studies appear to evaluate successfully oxygen transfer and cells suspension and experimental results show a dependence of cell growth on mean shear stress in the reactor.[122]

As an improvement of the basic rotor shape, a TCR featuring a lobed inner cylinder in conjugation with a membrane system for enhanced gas supply in the reactor was developed. This lobe appears to prevent bubble breakup, coalescence and foam formation, which are often liable for cell death. They applied this modified lobed reactor to investigate the influence of hydrodynamic stress on living mammalian cells by simulating values near the impeller of a stirred tank bioreactor (around 0.4 Pa). It was observed in this narrowly shear-stress distributed systems that cells actively changed their metabolism leading to increased lactate production while keeping the nutrients consumption constant.[65]

Further studies also aided by PIV and CFD simulations were done by Zhu et al. for the culture of rat bone marrow stroma cells in sponge-like structures, which verified the measured flow profiles and the distribution of the shear rate and stress over throughout the TCR. This study reports that moderate shear stresses (between 0.02 and 0.19 Pa) in the bioreactor enhanced the proliferation of rat bone marrow stroma cells 1.3 fold with respect to the generation in the static control while maintaining calcium deposition ability of the cells. Increasing to shear stresses of 0.24 Pa promoted the calcium deposition ability of the cells yet their proliferation was inhibited. Finally, larger values (above 0.24 Pa) resulted in declining both the cell count and ability to preserve calcium ions.[123]

Finally, yet another variation of the geometry of TCR was tested in a different study. In this case, a double gap Couette configuration was used to study the breakage of liposome vesicles, which is relevant to drug delivery. A scheme of the setup is shown in Figure 10, where two coaxial stationary cylinders form a ring filled with liquid and another cylindrical tube is introduced in the ring dividing it into two sections. This leaves a double gap geometry where two flows coexist: a Couette flow with the outer cylinder rotating and the inner cylinder stationary in the inner ring (between R1 and R2) and the corresponding opposite in the outer ring (between R3 and R4). The breakage of liposomes and their size in an aqueous suspension was studied over a range of shear rates. The change in size distributions increased concomitantly with the shear rate for a fixed time of shearing: the average diameter was found to be reduced continuously attaining at the highest shear rate (4,000 $s^{-1}$) a reduction of 38% after 6 h.[124]

### 4.4 | Polymer synthesis

The application of TCRs in polymer synthesis is mostly attributed to two characteristics. Firstly, the internal mixing of the vortices and the

15475905, 2021, 5, Downloaded from https://aiche.onlinelibrary.wiley.com/doi/10.1002/aic.17228, Wiley Online Library on [09/07/2024]. See the Terms and Conditions (https://onlinelibrary.wiley.com/terms-and-conditions) on Wiley Online Library for rules of use; OA articles are governed by the applicable Creative Commons License

high surface area to volume ratio of this reactor. This is an advantage especially when dealing with (highly) exothermic reactions, for example, polymerizations. Secondly, the controllable hydrodynamic behavior in combination with low shear forces lead to narrow particle size distributions and a precise control of the formed polymer particles.[125] Resulting from the excellent internal mixing properties, the Taylor-Couette reactor has been applied in a wide range of polymer reactions, like multi-phase reaction (e.g., emulsion polymerization), where excellent heat transfer and mixing are required. Table 6 shows a selection of polymer reactions that have been facilitated in a TCR, sorted by reaction type as well as substrate.

Woliński et al. used a continuously operated TCR in the polycondensation of bisphenol A with iso- and terephthaloyl chlorides using phase transfer catalysis. They further investigated the influence of the operating and reaction parameters on the conversion and the product properties. The authors could also show that a reduction of 90% of the original residence time is possible in comparison to a conventional CSTR.[126]

Oberhoff et al. describe in the patent currently held to BASF the use of a TCR for the mass polymerization of various substrates (e.g., n-butyl methacrylate).[127] Detailed investigations of the influence of the TCR fluid dynamics on conversion and polymer properties were conducted.

Furthermore, *Liu* and *Kind* investigated the influence of fluid dynamics on the polymer properties. A model was developed for the radical polymerization of methyl methacrylate that describes the influence of hydrodynamics on the monomer conversion in the reactor.[125] They were able to develop a correlation describing the mean molecular mass $M_w$ as a function of the Taylor and the first-order Damköhler number $Da_I$ (Equation (55)) and suggest a dimensionless correlation for the scale-up of the TCR.[128]

$$M_w = 66 \cdot 10^3 \cdot \left( Ta \cdot \sqrt{\frac{d}{r_i}} \right)^{-\left(1.82 \cdot 10^{-4} Da_I + 5.92 \cdot 10^{-2}\right)} \quad (55)$$

Kádár et al. investigated the observed phenomenon of the activation of the polymerization reaction by the hydrodynamic in the TCR. The authors also investigated the influence of the mixing properties in the reactor on the chemical reaction.[129,130] The study showed that the polymerization could be accelerated at higher *Ta* for low conversions, but only minor influence was observed for conversions above 30%.

Imamura et al. and Kataoka et al. investigated the two-phase emulsion polymerization of styrene in a Taylor-Couette reactor.[131,132] They could show that the low back-mixing of this reactor type yields higher monomer conversions and a more uniform particle size distribution than a comparable CSTR. They conclude that the TCR is very suitable as a reactor for polymer synthesis since particle coagulation is effectively prevented by the uniform shear forces.

Wei et al. Investigated the influence of the geometric reactor dimensions as well as operating conditions on the mixing properties in the TCR and correlated a "tank-in-series"-model. They could show that the monomer conversion as well as the particle count can be precisely controlled by a variation of the Taylor number.[133]

The possibility of using a TCR for process intensification was discussed by Rüttgers et al. The authors proved that under the right circumstances an increase in space–time-yield of up to 200 is possible when comparing a TCR to a semi-batch process.[134]

Xue et al. investigated the emulsion polymerization of vinyl acetate in a TCR, but observed an oscillating monomer conversion that was only slightly higher than in a comparable CSTR.[135] The authors concluded that the flow pattern in the TCR is not optimal for the polymerization of vinyl acetate, as the flow shows significant differences in the polymerization of styrene.

González et al. implemented the Taylor-Couette reactor in a number of polymerization reactions with varying combinations of substrates (e.g., methyl methacrylate, 2-ethyl hexylacrylate, butyl acrylate). In all investigated cases the TCR outperformed a comparable CSTR in terms of conversion metrics as well as particle characteristics.[136]

Kim et al. used a continuously operated TCR for the coating of carbon black particles with polyethylhexyl acrylate for application in displays. They could show that the TCR could deliver a better productivity as well as better product properties as a comparable batch reactor.[137] The particles coated with the TCR possessed a smaller and more uniform shape, which the authors attribute to the uniform hydrodynamic characteristics in the annular gap of the reactor. Furthermore, the authors could show that the particle size can be

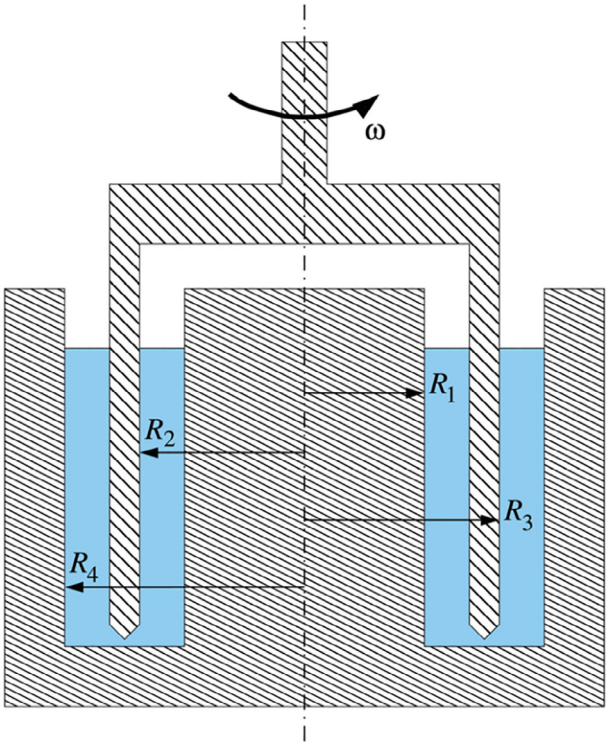


**FIGURE 10** Scheme of the double gap Couette geometry used by Pal et al.[124] Reprinted with permission from RSC Publishing. Copyright 2019 [Color figure can be viewed at wileyonlinelibrary.com]

15475905, 2021, 5, Downloaded from https://aiche.onlinelibrary.wiley.com/doi/10.1002/aic.17228, Wiley Online Library on [09/07/2024]. See the Terms and Conditions (https://onlinelibrary.wiley.com/terms-and-conditions) on Wiley Online Library for rules of use; OA articles are governed by the applicable Creative Commons License

precisely tuned by changing the axial flow and the rotational speed of the reactor.

The variety of reactions, substrates and investigated influencing characteristics in this chapter and Table 6 show, that the Taylor-Couette reactor is well suited for polymer reactions. In many cases, the TCR can deliver higher conversions and better product properties than a comparable CSTR. These characteristics are mostly attributed to the narrow residence time distribution as well as the intense, but uniform mixing properties in the annular gap.

## 4.5 | Crystallization and solid processing

In the precipitation and crystallization of solids, fluid dynamic variables like mixing intensity, reactor design and geometry have proven to hold a great influence on several parameters of interest, including crystal size distribution (CSD), internal microstructure, and morphology.[138] Compared with other configurations of crystallizers, micromixing times in TCRs do not depend that much on feed flow conditions but rather on the inner cylinder rotation. For all of this, the uniformity in the fluid dynamic conditions is one of the great advantages that TCRs offer for crystallization purposes.

The CSD and morphology of calcium carbonate precipitates have been studied evaluating the effect of Taylor vortices upon the reaction of $CO_2$ with $Ca(OH)_2$ in aqueous media. The morphological changes in the $CaCO_3$ generated were caused by the excess $Ca^{2+}$ ions, which is controlled by the interfacial transport of $CO_2$ (which is herein measured as a function of the rotating speed) and stoichiometric feed. It was hence observed that an increase of $Ca(OH)_2$ concentration and decreasing the interfacial transport rate, led to shifts from rhombohedrum to needle-shaped crystals. As for the size distribution, nucleation, and growth were rapidly completed at low axial positions (entry of the reactor), which were followed by agglomeration. Thus, the crystal size varied along the axis as a reciprocal function of the energy dissipated caused by the rotation of the cylinder, that is, when energy dissipation increased, agglomeration was inhibited by the turbulent force.[138]

Another study by Jung et al. followed some years later, where morphology and CSD were again assessed in a TCR and a stirred tank. The Taylor vortex promoted more homogeneous mixing leading to

**TABLE 6** Investigations of polymer reactions performed in a Taylor-Couette reactor

| Reaction type | Substrate | Topic/characteristic | Source |
|---|---|---|---|
| Radical polymerization | MMA | • Influence of fluid dynamics on monomer conversion | 125 |
| | | • Influence of fluid dynamics on polymer properties | 128 |
| | | • Activation of polycondensation by means of hydrodynamic parameters (batch), influence of hydrodynamics on monomer conversion, molecular weight distribution and viscosity (batch) | 130 |
| | | • Activation of polymerization by means of mixing properties | 129 |
| Poly-condensation | BPA | • Synthesis of polyarylates by interfacial polycondensation of bisphenol A with iso- and terephthaloyl chlorides using phase transfer catalysis | 126 |
| Mass-polymerization | Varying, for example, BMA | • Mass polymerization of several substrates | 127 |
| Emulsion-polymerization | Styrene | • Narrow molecular weight distribution, low shear forces, comparison of TCR with CSTR<br>• Optimization of hydrodynamics and operating conditions in the TCR<br>• Influence of the geometric and operating parameters on mixing properties, application of "tank in series" model<br>• Process intensification using TCR, TCR as chemical reactor | 131-134 |
| | VA | • Comparison of TCR with CSTR in the copolymerization of vinyl acetate with styrene | 133,135 |
| | Varying, for example, MMA | • Hybrid polymer synthesis, mini- and inverse microemulsion- polymerization, comparison with CSTR | 136 |
| Coating application | EHA | • Coating of "carbon black" for electrophoretic displays, synthesis of smaller and more uniform particles, comparison with batch reactor | 137 |

Abbreviations: BMA, butyl methacrylate; BPA, Bisphenol A; EHA, 2-ethyl hexylacrylate; MMA, methyl methacrylate; VA, vinyl acetate.

15475905, 2021, 5, Downloaded from https://aiche.onlinelibrary.wiley.com/doi/10.1002/aic.17228, Wiley Online Library on [09/07/2024]. See the Terms and Conditions (https://onlinelibrary.wiley.com/terms-and-conditions) on Wiley Online Library for rules of use; OA articles are governed by the applicable Creative Commons License

the generation of smaller particles with uniform shape along the reactor. On the other hand, precipitation in the stirred tank reactor led to the simultaneous production of cube and spindle-shaped solids at a high concentration of $Ca^{2+}$ ions, mostly due the locally non-homogeneous mixing intensity. Concerning CSD, the distribution was mainly bimodal, although the excess of $Ca^{2+}$ was key to decrease the mean size whereas stoichiometric concentrations produced more cubic structures.[139,140] Finally, one further paper reported on the effect of using monovalent salts with ions like $Na^+$, $K^+$, and $NH_4^+$ finding that the small radius ions, namely the two former, led to a change from regular rhombohedra to spindle-shaped crystals, whereas $NH_4^+$ is too large to be interstitially included in the crystal.[141]

The production of another bulk chemical like $BaSO_4$, with wide applications in paper coatings, pigments or radiocontrast agents, has also been reported in TCR devices. Experiments at three different axial flow rates under laminar flow (i.e., before the onset of instability) and vortex flow (i.e., after the onset of primary instability) proved that the conditions of the vortex has a great influence on the internal microstructure and morphology of the precipitates. In particular, flowrates at the onset of instability gave rise to crystalline sizes between 40 and 50 nm, although no trend was observed in laminar flow. Concerning the CSD, decreasing the residence time by increasing axial flow rate resulted in a decline of the crystal size both laminar and vortex flow. Remarkably, under vortex flow, an increase in axial flow resulted in even narrower CSD compared with laminar flow.[142]

Guanosine 5-Monophosphate (GMP) drowning-out crystallization was evaluated in a continuous TC setup following a drowning-out crystallization procedure. In such process, amorphous GMP is initially generated and subsequently transformed into hydrates through the consecutive dissolution of the amorphous structure followed by nucleation and growth. Because of the mixing promoted by the Taylor vortex both, the dissolution of amorphous GMP and growth of the crystal occur more easily. Comparing this procedure to mixed suspension mixed product removal (MSMPR) crystallization under equivalent conditions of rotation rate and feed concentration, the residence time was reduced up to five times using a TCR.[143]

The production of semiconductor materials has also been acknowledged in the scientific literature. An example would be the synthesis of quantum dot (QD) nanocrystals, for which TCR has proven an ingenious fluid dynamically controlled technology to obtain cadmium selenide QD nanocrystals with throughputs as high as 22,560 kg $day^{-1}$ $m^{-3}$ in space–time yield. As in the previous crystallization cases, a much narrower size distribution was attained compared with more conventional processes, such as the batch-type hot injection method.[144]

Further on semiconductors, a TCR was used to study the oxidation of graphite flakes and obtain graphite oxide, a precursor to graphene oxide. In this setup, mixing of graphite and oxidizing agents was successfully achieved via Taylor vortices, which reportedly shortened the synthesis of graphite oxide from hours to minutes.[145,146] The synthesis of this material and the level of oxidation reached were tested under different hydrodynamic flow regimes: Couette flow, Taylor vortex flow, wavy vortex flow as well as the primary and secondary instabilities between these. The results by AlAmer show that at the Taylor vortex flow condition not only the degree of oxidation increased, but also structurally more uniform graphite oxide was obtained compared with the other flows, where these features were less favorable. These two properties render this material more advantageous toward applications like energy storage and catalysis.[145]

The preparation of $MnO_2$/defect-free graphene nanocomposites with outstanding electrochemical properties has also been recently developed in a TCR. While not focusing so much on engineering aspects of the setup, it is demonstrated that under wavy vortex flow these nanocomposites can undergo fast shear exfoliation and be turned into ultrathin graphene sheets with the aid of ionic liquids to prevent their restacking.[147] Similarly, $RuO_2$/graphene sheets were synthesized also in the presence of ionic liquids in a TCR for use as selective oxidation catalysts with the same exfoliating properties of the Taylor flow being reported.[148]

The treatment of multiwalled carbon nanotube composites was performed in turbulent TC flow, whereby the vortex flow was able to achieve a uniform dispersion of nanotubes. The flow was able to debundle the highly entangled structures originally processing in a polymer matrix, for which the shear forces generated in this flow showed better results in exfoliation than the more traditional three-roll milling process used for this purpose.[149]

### 4.6 | Aggregation and flocculation of solids

There have also been a number of studies dealing with the aggregation and flocculation of already existing particles to reach different conformations or attain other size distributions. This procedure is of particular interest in water treatments, where the removal of fine solid particles in suspension is much facilitated when aggregation and change of size takes place.

Commonly, higher applied shear rates lead to lower aggregate diameters, narrower floc size distributions and higher fractal dimensions. In stirred tanks or during the transfer processes, aggregates undergo different shear rates owing to the inhomogeneity of hydrodynamics. These variations cause different steps of breakage and regrowth on the aggregate size and morphology.[38,150] In these regards, the controlled shear stresses that TC flows offer can be of great help for tuning the particle or floc sizes.

The flocculation of bentonite clay was performed in a TCR under different shear rates analyzing morphology parameters like the radius of gyration and circularity. Overall, the experimental results pointed out that flocs of similar sizes produced under different hydrodynamic flows have different shapes. The sizes are calibrated by the turbulence created since the double radius of gyration is close to Kolmogorov microscale; on the other hand, circularity appears to be greatly influenced by the rotation speed of the reactor.[151] In a different study, flocculation of bentonite was carried out aided by a commercially available cationic polyacrylamide. Here, enhanced growth rates and decreased fractal dimensions were observed for higher order flow states, leading to the conclusion that improved mass transfer of the

15475905, 2021, 5, Downloaded from https://aiche.onlinelibrary.wiley.com/doi/10.1002/aic.17228, Wiley Online Library on [09/07/2024]. See the Terms and Conditions (https://onlinelibrary.wiley.com/terms-and-conditions) on Wiley Online Library for rules of use; OA articles are governed by the applicable Creative Commons License

polymer flocculant and breakage at the edges of the flocs to more round morphologies occur, respectively.[152]

The aggregation and flocculation of latex particles was also analyzed through the monitoring of size and shape (circularity and convexity) of aggregates in sequenced growth-breakage-regrowth cycles. The investigation studied alternate steps alternating low and high shear rates in turbulent conditions and the conclusions were that the aggregate size distribution was controlled by the flow regime with shape distributions evolving throughout the sequential experiments. Nevertheless, the main finding of the study is the lack of correlation between the aggregate shape and the hydrodynamic regime. In fact, after multiple stages of breakage and regrowth, the aggregate shape reached a steady-state morphological distribution independent of aggregate size distribution and hydrodynamics.[38]

The biological floc size in activated sludge was assessed in a TC bioreactor rotating either the inner or the outer walls, and then compared against bubble-column sequencing batch reactors. In the experiments in the latter setup, the floc sizes did not show remarkable changes with shear rate or geometry, although in the TC bioreactor, the mean particle size decreased proportionally with increased hydrodynamic shear with the variation of size being smaller when the inner walls were rotating compared with the outer walls.[153]

## 5 | CONCLUSION

This overview has covered phenomenological aspects of the Taylor-Couette flow, which takes place in the annular gap between a rotating inner cylinder in a cylindrical shell. After setting the fundamentals of the Taylor-Couette flow, a series of characterizing variables and design elements are herein presented together with an extensive summary of design rules and correlations developed throughout the years for residence time distribution, mass and heat transport properties, and multiphase mixing. In addition, modifications to the geometry of the inner cylinder are discussed that significantly influence the shear rate and residence time within the apparatus.

Table 7 compiles and discusses succinctly on the advantages and challenges of the TCR presented throughout this document. Through the choice of the design parameters of the reactor body as well as the operating conditions like the rotational speed, the TCR has proven very versatile for a large variety of different applications, especially

**TABLE 7** Concluding remarks on the advantages and challenges of a TCR

| Advantages | Challenges |
|---|---|
| **Fine tuning of shear stress**<br>• Important in, for example, bioprocesses and waste water treatment<br>• Determined by flow pattern and rotor design<br>• Vortices of Taylor-Couette flow provide low and uniform shear forces<br>• Lobed rotor and large gaps reduce shear forces while rotor design with cavitation holes increases shear stress<br>**Fine tuning of residence time**<br>• Beneficial for the control of particle sizes in processes such as crystallization and polymerization, as well as for long reaction times<br>• RTD of TCR approaches that of a cascade of CSTRs with each vortex being fully backmixed<br>• Mixing conditions can be set nearly independently from axial flow (depends mainly on Ta)<br>• Ribbed rotor (or TCDC) further stabilizes vortices, reduces axial dispersion and increases degree of micromixing<br>**Uniform mixing**<br>• Important for, for example, suspension of particles, debundling of highly entangled nanotube composites, handling of cells and enzymes, photocatalysis<br>**High surface to volume ratio**<br>• Advantageous, for example, when dealing with exothermic reactions where heat needs to be removed, such as polymerizations<br>**Mixing of non-Newtonian fluids**<br>• Such fluids appear, for example, in food processing, bioprocesses and polymerization<br>• Many recent studies show the progress in understanding how, for example, shear-thinning affects the flow structures. However, as the transition of flow patterns is not sharp as with Newtonian fluids, the experimental determination of for example, critical Taylor numbers is aggravated<br>• More studies in this field are required to unlock the full potential of TCRs in this field | **Complexity of available flow regimes**<br>• Various flow regimes can be formed in the annular gap, with significantly different flow conditions and shapes<br>• Number of flow regimes increases if both rotor and shell are rotating<br>• While scientifically of interest, the industrial practicability of the many accessible flow regimes has yet to be shown<br>• Axial dispersion coefficient may vary by a factor of two in the wavy flow regime, giving importance to how the flow pattern was accessed<br>**Flow patterns of TCR are not generally superior to traditional ones**<br>• While the use of TCR is beneficial in many applications as discussed in this review, this is not always the case, for example:<br>• Polymerization of vinyl acetate shows an oscillating monomer conversion only slightly higher than in a comparable CSTR<br>• Accumulation of homogeneous palladium catalyst at the (heated) inner cylinder may lead to catalyst deactivation<br>**Lack of reports on high pressure applications**<br>• High aspect ratios in the reactor design imply a reduced diameter for a given reaction volume, resulting in smaller required wall thicknesses for a given design pressure<br>• However, in the studies presented in this work, the pressure did not exceed 4 bar(g), presumably due to the sealings and bearings of the rotor being more complex to seal against pressure<br>**Lack of reports on industrial application**<br>• The lack of reports may be due to the difficult scale-up of the reactor, especially when considering the sealings, bearings, and mechanical drive required to move a large-scale rotor<br>• A scale-up by numbering up lessens the advantage over a cascade of stirred tanks, as in both cases multiple reactors are required<br>• Rotating parts are prone to attrition, which is an important factor for industrial processes that oftentimes have many operating hours per year |

15475905, 2021, 5, Downloaded from https://aiche.onlinelibrary.wiley.com/doi/10.1002/aic.17228, Wiley Online Library on [09/07/2024]. See the Terms and Conditions (https://onlinelibrary.wiley.com/terms-and-conditions) on Wiley Online Library for rules of use; OA articles are governed by the applicable Creative Commons License

when uniform mixing and the ability to tune the residence time distribution and shear forces are advantageous. Among the applications are chemical and biochemical reactions promoted by catalysts of different nature as well as processes that include the handling of solids, including cell growth, crystallization, and aggregation-flocculations. The Taylor-Couette reactor offers clear advantages in these operations. Of special relevance seem to be applications where solids partake since the controllable and uniform shear forces in this design lead to a controlled disruption and hence the production of solid particles with narrow size distributions and controlled morphologies. In addition, for the growth of microorganisms like cells, the fluid flow is capable of rapidly and gently shuttling them. The narrow residence time distribution obtained has proven to help reaction times in homogeneously catalyzed reactions. And for polymer synthesis, high specific surface areas are supplied, which facilitate heat transfer, which is important in this type of exothermic reactions.

However, while the TCR is applied in lab-scale experiments, reports on industrial applications are scarce as discussed in Table 7. The required high diameter ratio of above $\Lambda = 0.5$ significantly further reduces the available volume for reactions to take place in relation to the total reactor volume. The limitation that fluid injection may only take place from either end of the reactor further limits the axial throughput, which is especially disadvantageous for a scale-up. A solution to this has only recently emerged with the introduction of radial fluid injection through the inner rotor. Moreover, the strong influence of the design parameters on the reactor's performance reduce the comparability of different studies, further aggravating the applicability of the results for design and scale-up. This is also evident by the axial dispersion coefficient depending not only on the momentary Taylor number, but also on the ramp function used to attain the flow pattern.

## 6 | OUTLOOK

Given the advantages of the TCR, there appears to be genuine potential for the application of this reactor in other operations dealing with solid processing, water treatment or even multiphasic reactions, where different Taylor flow regimes could exert an effective control of transport properties. Based on its flow, the Taylor-Couette reactor is a special design that offers some interesting advantages in comparison to commonly used stirred tanks, tubular reactors, or more modern process intensified contactors. Apart from a controllable residence time distribution, this configuration allows fine-tuning of mass and heat transfer as well as its gentle but efficient mixing. Therefore, the hydrodynamics within the reactor can be specifically tailored for a given task. While the Taylor-Couette reactor is significantly more complex to design and control than traditional reactor designs, it has a great potential as shown in the many applications discussed in this review.

A great opportunity for the use of the TCR lies in the mixing of non-Newtonian fluids as evident by the very recent advancements in this field. However, so far only the flow of non-Newtonian fluids itself has been in the focus of studies, with applications in this area being mostly limited to polymerization. The possible applications include food processing, polymerization processes, bioprocesses, and water treatment. Here, the relatively small gap of the TCR counteracts the distribution of the velocity and therefore that of the viscosity while enabling a controlled mixing with a high energy dissipation rate.

### ACKNOWLEDGMENT

The Max Planck Society is gratefully acknowledged for funding. Open Access funding enabled and organized by Projekt DEAL.

### AUTHOR CONTRIBUTIONS

**Marco Schrimpf:** Data curation; formal analysis; writing-original draft; writing-review & editing. **Jesus Esteban:** Conceptualization; data curation; supervision; validation; writing-original draft; writing-review & editing. **Arno Behr:** Conceptualization; funding acquisition. **Helge Warmeling:** Writing-original draft. **Tobias Färber:** Writing-original draft. **Andreas Vorholt:** Conceptualization; funding acquisition; project administration; resources; supervision; writing-original draft; writing-review & editing.

### SYMBOLS

**Greek**

| | |
|---|---|
| $\alpha$ | Heat transfer coefficient, $Wm^{-2}\,K^{-1}$ |
| $\beta$ | Coefficient of thermal expansion, $K^{-1}$ |
| $\Gamma$ | Aspect ratio $\Gamma = \frac{H}{d}$ |
| $\gamma$ | Shear stress, Pa |
| $\eta$ | Dynamic viscosity,Pas |
| $\Lambda$ | Diameter ratio $\Lambda = \frac{d_i}{d_o}$ |
| $\lambda$ | Thermal heat conductivity, $Wm^{-1}\,K^{-1}$ |
| $\nu$ | Kinematic viscosity, $m^2s^{-1}$ |
| $\rho$ | Density, $kgm^{-3}$ |
| $\sigma$ | Interfacial tension, $Nm^{-1}$ |
| $\phi$ | Volumetric phase fraction |
| $\omega$ | Angular velocity, $rads^{-1}$ |

**Latin**

| | |
|---|---|
| b | Specific length, m |
| c | Concentration, $molm^{-3}$ |
| $C_j$ | Constant number j |
| $c_p$ | Heat capacity, $JK^{-1}$ |
| D | Diffusion coefficient, $m^2s^{-1}$ |
| $D_z$ | Dispersion coefficient, $m^2s^{-1}$ |
| $Da_I$ | First order Damköhler number |
| d (no index) | Gap width $d = \frac{1}{2}\cdot(d_i - d_o)$, m |
| d (with index) | Diameter, m |
| $d_{32}$ | Sauter mean diameter |
| e | Radii of the lobed cylinders, m |
| F | Cumulative function |
| Fr | Froude number $Fr = \frac{d_D\omega^2}{g}$ |
| g | Gravitational acceleration, $ms^{-2}$ |
| G | Dimensionless torque |
| Gr | Grashof number $Gr = \frac{g\beta\Delta T d^3}{\nu^2}$ |
| H | Height, m |
| $k_L$ | Mass transport coefficient, $ms^{-1}$ |

15475905, 2021, 5, Downloaded from https://aiche.onlinelibrary.wiley.com/doi/10.1002/aic.17228, Wiley Online Library on [09/07/2024]. See the Terms and Conditions (https://onlinelibrary.wiley.com/terms-and-conditions) on Wiley Online Library for rules of use; OA articles are governed by the applicable Creative Commons License

| | |
|---|---|
| m | Exponent for a power law |
| Mo | Morton number $Mo = \frac{g \cdot \eta^4 \cdot \Delta\rho}{\rho_c \cdot \sigma^3}$ |
| $M_w$ | Mean molecular mass, $kgmol^{-1}$ |
| n | Rotation rate of rotor, $s^{-1}$ |
| Nu | Nusselt number $Nu = \frac{\alpha \cdot 2d}{\lambda_l}$ |
| Pe | Péclet number $Pe = \frac{H \cdot u_{ax}}{D_z}$ |
| Pr | Prandtl number $Pr = \frac{\nu}{\lambda}$ |
| $PV^{-1}$ | Specific energy input, $Jm^{-3}$ |
| $\dot{q}$ | Rate of heat transfer per unit area, $Js^{-1}\ m^{-2}$ |
| Re | Reynolds number $Re_{ax} = \frac{u_{ax} d}{\nu}$ |
| Sc | Schmidt number $Sc = \frac{\nu}{D_i}$ |
| Sh | Sherwood number $Sh = \frac{k_l \cdot b}{D_i}$ |
| Ta | Taylor number $Ta = \frac{\omega r_i d}{\nu}$ |
| t | Time, s |
| u | Velocity, $ms^{-1}$ |
| We | Weber number $We = \frac{\rho_c (\omega r_i)^2 d}{\sigma}$ |

**Abbreviations**

| | |
|---|---|
| ax | axial |
| c | continuous phase |
| CFD | computational fluid dynamics |
| CSD | crystal size distribution |
| CSTR | continuous stirred tank reactor |
| d | dispersed phase |
| D | disk |
| eff | effective |
| i | inner/component i |
| inj | injection |
| K | pure conductive heat transfer |
| L | lobed |
| l | liquid |
| max | maximal |
| min | minimal |
| O | outer |
| PFR | plug flow reactor |
| R | reactor |
| QD | quantum dots |
| RTD | residence time distribution |
| TCDC | Taylor-Couette disk contactor |
| TCR | Taylor-Couette reactor |
| TMS | thermomorphic solvent system |
| w | wall |

## ORCID

*Marco Schrimpf* https://orcid.org/0000-0003-1847-7854
*Jesús Esteban* https://orcid.org/0000-0003-3729-5378
*Helge Warmeling* https://orcid.org/0000-0002-5516-4470
*Andreas J. Vorholt* https://orcid.org/0000-0001-9302-2273

## REFERENCES

1. Khalde CM, Pandit AV, Sangwai JS, Ranade VV. Flow, mixing, and heat transfer in fluidic oscillators. *Can J Chem Eng*. 2019;97(2):542-559.
2. McDonough JR, Phan AN, Harvey AP. Rapid process development using oscillatory baffled mesoreactors - a state-of-the-art review. *Chem Eng J*. 2015;265:110-121.
3. Carpenter J, Badve M, Rajoriya S, George S, Saharan VK, Pandit AB. Hydrodynamic cavitation: an emerging technology for the intensification of various chemical and physical processes in a chemical process industry. *Rev Chem Eng*. 2017;33(5):433-468.
4. Chakravorty A. Process intensification by pulsation and vibration in miscible and immiscible two component systems. *Chem Eng Process*. 2018;133:90-105.
5. Schrimpf M, Esteban J, Rösler T, Vorholt AJ, Leitner W. Intensified reactors for gas-liquid-liquid multiphase catalysis: from chemistry to engineering. *Chem Eng J*. 2019;372:917-939.
6. Suryawanshi PL, Gumfekar SP, Bhanvase BA, Sonawane SH, Pimplapure MS. A review on microreactors: reactor fabrication, design, and cutting-edge applications. *Chem Eng Sci*. 2018;189:431-448.
7. Tanimu A, Jaenicke S, Alhooshani K. Heterogeneous catalysis in continuous flow microreactors: a review of methods and applications. *Chem Eng J*. 2017;327:792-821.
8. Esteban J, Warmeling H, Vorholt AJ. An approach to chemical reaction engineering and process intensification for the lean aqueous Hydroformylation using a jet loop reactor. *Chem Ing Tech*. 2019;91(5):560-566.
9. Mallock A. Determinatino of the viscosity of water. *Proc R Soc Lond*. 1888;A45:126-126.
10. Mallock A. Experiments on fluid viscosity. *Philos Trans R Soc Lond*. 1896;A187:41-41.
11. Couette M. Études sur le frottement des liquides. *Ann Chim Phys*. 1890;21:433-433.
12. Taylor GI. Stability of a viscous liquid contained between two rotating cylinders. *Philos Trans R Soc A Math Phys Eng Sci*. 1923;223(605-615):289-343.
13. Andereck CD, Dickman R, Sweinney HL. New flows in a circular Couette system with co-rotating cylinders. *Phys Fluids*. 1983;26(6):1395-1395.
14. Andereck CD, Liu SS, Swinney HL. Flow regimes in a circular Couette system with independently rotating cylinders. *J Fluid Mech*. 1986;164:155-183.
15. Coles D. Transition in circular Couette flow. *J Fluid Mech*. 1965;21(03):385-385, 425.
16. Snyder HA. Stability of rotating Couette flow. *I Asymme Waveform Phys Fluid*. 1968;11(4):728-728.
17. Snyder HA. Waveforms in rotating Couette flow. *Int J Nonlin Mech*. 1970;5(4):659-685.
18. Kataoka K, Doi H, Kongo T, Futugawa M. Ideal plug-flow properties of taylor vortex flow. *J Chem Eng Jpn*. 1975;8(6):472-476.
19. Pudjinono OI, Tavare NS, Garside J, Nigam KDP. Residence time distribution from a continuous Couette flow device. *Chem Eng J*. 1992;48:101-101, 110.
20. Gu ZH, Fahidy TZ. Characteristics of Taylor vortex structure in combined axial and rotating flow. *Can J Chem Eng*. 1985;63(5):710-715.
21. Moore CMV, Cooney CL. Axial dispersion in Taylor-Couette flow. *AIChE J*. 1995;41(3):723-727.
22. Donnelly RJ. Taylor-Couette flow: the early days. *Phys Today*. 1991;44(11):32-39.
23. Ohenoja M, Boodhoo K, Reay D, Paavola M, Leiviskä K. Process control in intensified continuous solids handling. *Chem Eng Process*. 2018;131:59-69.
24. Beaudoin G, Jaffrin MY. Plasma filtration in Couette flow membrane devices. *Artif Organs*. 1989;13(1):43-51.
25. Eggert A, Kogl T, Arlt W, Jupke A. Computer tomographic detection of the liquid-liquid mixing and separation within the annular centrifugal contactor/extractor. *Chem Eng Res Des*. 2019;142:143-153.

15475905, 2021, 5, Downloaded from https://aiche.onlinelibrary.wiley.com/doi/10.1002/aic.17228, Wiley Online Library on [09/07/2024]. See the Terms and Conditions (https://onlinelibrary.wiley.com/terms-and-conditions) on Wiley Online Library for rules of use; OA articles are governed by the applicable Creative Commons License

26. Eggert A, Sibirtsev S, Menne D, Jupke A. Liquid-liquid centrifugal separation - new equipment for optical (photographic) evaluation at laboratory scale. *Chem Eng Res Des*. 2017;127:170-179.
27. Nakase M, Matsuzawa Y, Takeshita K. Continuous separation of molybdenum and zirconium from simulated high-level liquid waste with a Taylor-Couette contactor. *J Nucl Sci Technol*. 2018;55(11):1317-1323.
28. Nakase M, Matsuzawa Y, Takeshita K. Modified flow geometry for higher extraction performance with a liquid-liquid centrifugal contactor with Taylor vortices. *J Nucl Sci Technol*. 2018;55(8):829-837.
29. Fardin MA, Perge C, Taberlet N. "The hydrogen atom of fluid dynamics" – introduction to the Taylor–Couette flow for soft matter scientists. *Soft Matter*. 2014;10(20):3523-3535.
30. Vedantam S, Joshi JB. Annular centrifugal contactors - A review. *Chem Eng Res Des*. 2006;84(A7):522-542.
31. Majji MV, Morris JF. Inertial migration of particles in Taylor-Couette flows. *Phys Fluids*. 2018;30(3):033303.
32. Nemri M, Climent E, Charton S, Lanoë J-Y, Ode D. Experimental and numerical investigation on mixing and axial dispersion in Taylor–Couette flow patterns. *Chem Eng Res Des*. 2013;91(12):2346-2354.
33. Nemri M, Charton S, Climent E. Mixing and axial dispersion in Taylor–Couette flows: the effect of the flow regime. *Chem Eng Sci*. 2016;139:109-124.
34. Wereley ST, Lueptow RM. Velocity field for Taylor–Couette flow with an axial flow. *Phys Fluids*. 1999;11(12):3637-3649.
35. Richter O, Hoffmann H, Kraushaar-Czarnetzki B. Effect of the rotor shape on the mixing characteristics of a continuous flow Taylor-vortex reactor. *Chem Eng Sci*. 2008;63(13):3504-3513.
36. Reinke P, Schmidt M, Beckmann T. The cavitating Taylor-Couette flow. *Phys Fluids*. 2018;30(10):104101.
37. Murai Y, Tasaka Y, Oishi Y, Takeda Y. Modal switching of bubbly Taylor–Couette flow investigated by particle tracking velocimetry. *Exp Fluids*. 2018;59(11):164.
38. Guérin L, Coufort-Saudejaud C, Liné A, Frances C. Dynamics of aggregate size and shape properties under sequenced flocculation in a turbulent Taylor-Couette reactor. *J Colloid Interface Sci*. 2017;491:167-178.
39. Lueptow RM, Docter A, Min K. Stability of axial flow in an annulus with a rotating inner cylinder. *Phys Fluids A-Fluid*. 1992;4(11):2446-2455.
40. Kataoka K. *Taylor vortices and instabilities in circular Couette flow*. Houston: Gulf Publishing; 1986.
41. Aksamija E, Weinländer C, Sarzio R, Siebenhofer M. The Taylor-Couette disc contactor: a novel apparatus for liquid/liquid extraction. *Sep Sci Technol*. 2015;50(January):2844-2852.
42. Giordano RLC, Giordano RC, Prazeres DMF, Cooney CL. Analysis of a Taylor–Poiseuille vortex flow reactor — II: reactor modeling and performance assessment using glucose-fructose isomerization as test reaction. *Chem Eng Sci*. 2000;55(18):3611-3626.
43. Gollub JP, Swinney HL. Onset of turbulence in a rotating fluid. *Phys Rev Lett*. 1975;35(14):927-930.
44. Esser A, Grossmann S. Analytic expression for Taylor–Couette stability boundary. *Phys Fluids*. 1996;8(7):1814-1819.
45. Recktenwald A, Lücke M, Müller HW. Taylor vortex formation in axial through-flow: linear and weakly nonlinear analysis. *Phys Rev E*. 1993;48(6):4444-4454.
46. Masuda H, Horie T, Hubacz R, Ohta M, Ohmura N. Prediction of onset of Taylor-Couette instability for shear-thinning fluids. *Rheol Acta*. 2017;56(2):73-84.
47. Bahrani SA, Nouar C, Neveu A, Becker S. Transition to chaotic Taylor-Couette flow in shear-thinning fluids 2015.
48. Topayev S, Nouar C, Bernardin D, Neveu A, Bahrani SA. Taylor-vortex flow in shear-thinning fluids. *Phys Rev E*. 2019;100(2):023117.
49. Escudier MP, Gouldson IW, Jones DM. Taylor vortices in Newtonian and shear-thinning liquids. *Proc Mathemat Phys Sci*. 1995;449(1935):155-176.
50. Cagney N, Balabani S. Taylor-Couette flow of shear-thinning fluids. *Phys Fluids*. 2019;31(5):053102.
51. Elçiçek H, Güzel B. Effect of shear-thinning behavior on flow regimes in Taylor–Couette flows. *J Non-Newtonian Fluid Mech*. 2020;279:104277.
52. Cagney N, Balabani S. Influence of shear-thinning rheology on the mixing dynamics in Taylor-Couette flow. *Chem Eng Technol*. 2019;42(8):1680-1690.
53. Masuda H, Yoshida S, Horie T, Ohmura N, Shimoyamada M. Flow dynamics in Taylor–Couette flow reactor with axial distribution of temperature. *AIChE J*. 2018;64(3):1075-1082.
54. Snyder HA. Change in wave-form and mean flow associated with wavelength variations in rotating Couette flow. Part 1. *J. Fluid Mech*. 1969;35(02):337-337, 352.
55. Jones CA. Nonlinear Taylor vortices and their stability. *J Fluid Mech*. 1981;102(1):249-249.
56. Jones CA. The transition to wavy vortices. *J Fluid Mech*. 1985;157(1985):13-15.
57. DiPrima RC, Eagles PM, Ng BS. The effect of radius ratio on the stability of Couette flow and Taylor vortex flow. *Phys Fluids*. 1984;27(10):2403-2411.
58. Chouippe A, Climent E, Legendre D, Gabillet C. Numerical simulation of bubble dispersion in turbulent Taylor-Couette flow. *Phys Fluids*. 2014;26(4):043304.
59. Ostilla-Mónico R, Huisman SG, Jannink TJG, et al. Optimal Taylor–Couette flow: radius ratio dependence. *J Fluid Mech*. 2014;747:1-29.
60. Grafschafter A, Aksamija E, Siebenhofer M. The Taylor-Couette disc contactor. *Chem Eng Technol*. 2016;39(11):2087-2095.
61. Wilkinson NA, Dutcher CS. Axial mixing and vortex stability to in situ radial injection in Taylor–Couette laminar and turbulent flows. *J Fluid Mech*. 2018;854:324-347.
62. Wilkinson N, Dutcher CS. Taylor-Couette flow with radial fluid injection. *Rev Sci Instrum*. 2017;88(8):083904.
63. Behr A, Färber T. Application of a Taylor-Couette reactor in homogeneous catalysis. *Chem Ing Trans*. 2015;43:835-840.
64. Soos M, Wu H, Morbidelli M. Taylor-Couette unit with a lobed inner cylinder cross section. *AIChE J*. 2007;53(5):1109-1120.
65. Sorg R, Tanzeglock T, Soos M, et al. Minimizing hydrodynamic stress in mammalian cell culture through the lobed Taylor-Couette bioreactor. *Biotechnol J*. 2011;6(12):1504-1515.
66. Forney LJ, Pierson JA, Giorges A. Photon absorption in modified Taylor—Couette flow: theory and experiment. *Ind Eng Chem Res*. 2005;44(14):5193-5198.
67. Lathrop DP, Fineberg J, Swinney HL. Transition to shear-driven turbulence in Couette-Taylor flow. *Phys Rev A*. 1992;46(10):6390-6405.
68. Rochex A, Godon J, Bernet N, Escudie R. Role of shear stress on composition, diversity and dynamics of biofilm bacterial communities. *Water Res*. 2008;42(20):4915-4922.
69. Sobolík V, Jirout T, Havlica J, Kristiawan M. Wall shear rates in taylor vortex flow. *J Appl Fluid Mech*. 2011;4(2):25-31.
70. Grafschafter A, Rudelstorfer G, Siebenhofer M. Hydraulics and operation performance of TCDC-extractors. *Chem Ing Tech*. 2018;90(6):864-871.
71. Dherbécourt D, Charton S, Lamadie F, Cazin S, Climent E. Experimental study of enhanced mixing induced by particles in Taylor–Couette flows. *Chem Eng Res Des*. 2016;108:109-117.
72. Rida Z, Cazin S, Lamadie F, Dherbécourt D, Charton S, Climent E. Experimental investigation of mixing efficiency in particle-laden Taylor–Couette flows. *Exp Fluids*. 2019;60(4):61.
73. Fogler HS. *Elements of chemical reaction engineering*. Vol 4. Prentice Hall: Upper Saddler River; 2005.

15475905, 2021, 5, Downloaded from https://aiche.onlinelibrary.wiley.com/doi/10.1002/aic.17228, Wiley Online Library on [09/07/2024]. See the Terms and Conditions (https://onlinelibrary.wiley.com/terms-and-conditions) on Wiley Online Library for rules of use; OA articles are governed by the applicable Creative Commons License

74. Levenspiel O. *Chemical reaction engineering*. 3rd ed. Hoboken: Wiley; 1998.
75. Mecklenburgh JC. Backmixing and design: a review. *Trans Inst Chem Eng*. 1974;52:180-180.
76. Resende MM, Vieira PG, Sousa R Jr, Giordano RLC, Giordano RC. Estimation of masstransfer parameters in a Taylor-Couette Poiseuille. *Braz J Chem Eng*. 2003;21(2):175-184.
77. Tamhane TV, Joshi JB, Kamachi Mudali U, Natarajan R, Patil RN. Axial mixing in annular centrifugal extractors. *Chem Eng J*. 2012; 207–208:462-472.
78. Whitman WG. The two-film theory of gas absorption. *Chem Metall Eng*. 1923;29(4):146-146.
79. Kataoka K, Doi H, Komai T. Heat/mass transfer in Taylor vortex flow with constant axial flow rates. *Int J Heat Mass Transf*. 1977;20(1): 57-63.
80. Srinivasan R, Jayanti S, Kannan A. Effect of Taylor vortices on mass transfer from a rotating cylinder. *AIChE J*. 2005;51(11):2885-2898.
81. Qiao J, Yan W-C, Teoh JH, Tong YW, Wang C-H. Experimental and computational studies of oxygen transport in a Taylor-Couette bioreactor. *Chem Eng J*. 2018;334:1954-1964.
82. Gao X, Kong B, Ramezani M, Olsen MG, Vigil RD. An adaptive model for gas-liquid mass transfer in a Taylor vortex reactor. *Int J Heat Mass Transf*. 2015;91:433-445.
83. Ramezani M, Kong B, Gao X, Olsen MG, Vigil RD. Experimental measurement of oxygen mass transfer and bubble size distribution in an air–water multiphase Taylor–Couette vortex bioreactor. *Chem Eng J*. 2015;279:286-296.
84. Ramezani M, Legg MJ, Haghighat A, Li Z, Vigil RD, Olsen MG. Experimental investigation of the effect of ethyl alcohol surfactant on oxygen mass transfer and bubble size distribution in an air-water multiphase Taylor-Couette vortex bioreactor. *Chem Eng J*. 2017;319: 288-296.
85. Farzad R, Puttinger S, Pirker S, Schneiderbauer S. Experimental investigation of liquid-liquid system drop size distribution in Taylor-Couette flow and its application in the CFD simulation. *EPJ Web of Conferences*. 2017;143:2021-2021.
86. Grafschafter A, Siebenhofer M. Design rules for the Taylor-Couette disc contactor. *Chem Ing Tech*. 2017;89(4):409-415.
87. Ho CY, Nardacci JL, Nissan AH. Heat transfer characteristics of fluids moving in a Taylor system of vortices. Part I.NPr= I. *AIChE J*. 1964;10(2):194-197.
88. Ho CY, Nardacci JL, Nissan AH. Heat transfer characteristics of fluids moving in a Taylor system of vortices. Part II. NPr ≠ I. *AIChE J*. 1964;10(2):197-202.
89. Aoki H, Nohira H, Arai H. Convective heat transfer in an annulus with an inner rotating cylinder. *Bullet JSME*. 1967;10(39): 523-532.
90. Donne MD, Meerwald E. Experimental local heat-transfer and average friction coefficients for subsonic turbulent flow of air in an annulus at high temperatures. *Int J Heat Mass Transf*. 1966;9(12): 1361-1376.
91. Simmers DA, Coney JER. A Reynolds analogy solution for the heat transfer characteristics of combined Taylor vortex and axial flows. *Int J Heat Mass Transf*. 1979;22(5):679-689.
92. Torii S, Yang W-J. Turbulent flow and heat transfer in circular Couette flows in concentric annulus. *Int J Rotat Mach*. 1998;4(1): 35-48.
93. Hosain ML, Bel Fdhila R, Rönnberg K. Taylor-Couette flow and transient heat transfer inside the annulus air-gap of rotating electrical machines. *Appl Energy*. 2017;207:624-633.
94. Kedia R, Hunt ML, Colonius T. Numerical simulations of heat transfer in Taylor-Couette flow. *J Heat Transf*. 1998;120(1):65-65, 71.
95. Lancial N, Torriano F, Beaubert F, Harmand S, Rolland G. Taylor-Couette-Poiseuille flow and heat transfer in an annular channel with a slotted rotor. *Int J Therm Sci*. 2017;112:92-103.
96. Lopez JM, Marques F, Avila M. Conductive and convective heat transfer in fluid flows between differentially heated and rotating cylinders. *Int J Heat Mass Transf*. 2015;90:959-967.
97. Fénot M, Bertin Y, Dorignac E, Lalizel G. A review of heat transfer between concentric rotating cylinders with or without axial flow. *Int J Therm Sci*. 2011;50(7):1138-1155.
98. Färber T, Schulz R, Riechert O, et al. Different recycling concepts in the homogeneously catalysed synthesis of terpenyl amines. *Chem Eng Process Process Intensif*. 2015;98:22-31.
99. Färber T, Riechert O, Zeiner T, Sadowski G, Behr A, Vorholt AJ. Homogeneously catalyzed hydroamination in a Taylor–Couette reactor using a thermormorphic multicomponent solvent system. *Chem Eng Res Des*. 2016;112:263-273.
100. Dreimann JM, Faßbach TA, Fuchs S, et al. Vom Laborkuriosum zum kontinuierlichen Prozess: Die Entwicklung thermomorpher Lösungsmittelsysteme. *Chem Ing Tech*. 2017;89(3):252-262.
101. Sczechowski JG, Koval CA, Noble RD. A Taylor vortex reactor for heterogeneous photocatalysis. *Chem Eng Sci*. 1995;50(20):3163-3173.
102. Sengupta TK, Kabir MF, Ray AK. A Taylor vortex photocatalytic reactor for water purification. *Ind Eng Chem Res*. 2001;40(23):5268-5281.
103. Subramanian M, Kannan A. Photocatalytic degradation of phenol in a rotating annular reactor. *Chem Eng Sci*. 2010;65(9):2727-2740.
104. Kabir MF, Ray AK. Performance enhancement of a chemical reactor utilizing flow instability. *J Chem Technol Biotechnol*. 2003;78(2–3): 314-320.
105. Forney LJ, Pierson JA. Optimum photolysis in Taylor-Couette flow. *AIChE J*. 2003;49(3):727-733.
106. Forney LJ, Pierson JA. Photolytic reactors: similitude in Taylor–Couette and channel flows. *AIChE J*. 2003;49(5):1285-1292.
107. Dutta PK, Ray AK. Experimental investigation of Taylor vortex photocatalytic reactor for water purification. *Chem Eng Sci*. 2004;59 (22–23):5249-5259.
108. Haim D, Pismen LM. Performance of a photochemical reactor in the regime of Taylor-Görtler vortical flow. *Chem Eng Sci*. 1994;49(8): 1119-1129.
109. Muller A, Orlowska M, Knorr M, Stahl MR, Greiner R, Koutchma T. Actinometric and biodosimetric evaluation of UV-C dose delivery in annular, Taylor-Coutte and coiled tube continuous systems. *Food Sci Technol Int*. 2017;23(3):222-234.
110. Ye Z, Forney LJ, Koutchma T, Giorges AT, Pierson JA. Optimum UV disinfection between concentric cylinders. *Ind Eng Chem Res*. 2008; 47(10):3444-3452.
111. Forney LJ, Ye Z, Koutchma T. UV disinfection of *E. coli* between concentric cylinders: effects of the boundary layer and a Wavy Wall. *Ozone Sci Eng*. 2008;30(6):405-412.
112. Giorges ATG, Pierson JA, Forney LJ. Effect of reactor length on the disinfection of fluids in Taylor–Couette Photoreactor. *Ind Eng Chem Res*. 2008;47(19):7490-7495.
113. Kong B, Shanks JV, Vigil RD. Enhanced algal growth rate in a Taylor vortex reactor. *Biotechnol Bioeng*. 2013;110(8):2140-2149.
114. Gao X, Kong B, Vigil RD. Characteristic time scales of mixing, mass transfer and biomass growth in a Taylor vortex algal photobioreactor. *Bioresour Technol*. 2015;198:283-291.
115. Gao X, Kong B, Vigil RD. Comprehensive computational model for combining fluid hydrodynamics, light transport and biomass growth in a Taylor vortex algal photobioreactor: Lagrangian approach. *Bioresour Technol*. 2017;224:523-530.
116. Gao X, Kong B, Vigil RD. Comprehensive computational model for combining fluid hydrodynamics, light transport and biomass growth in a Taylor vortex algal photobioreactor: Eulerian approach. *Algal Res*. 2017;24:1-8.
117. Resende MM, Vieira PG, Sousa R Jr, Giordano RLC, Giordano RC. Estimation of mass transfer parameters in a Taylor-Couette-Poiseuille heterogeneous reactor. *Braz J Chem Eng*. 2004;21(2):175-184.


15475905, 2021, 5, Downloaded from https://aiche.onlinelibrary.wiley.com/doi/10.1002/aic.17228, Wiley Online Library on [09/07/2024]. See the Terms and Conditions (https://onlinelibrary.wiley.com/terms-and-conditions) on Wiley Online Library for rules of use; OA articles are governed by the applicable Creative Commons License

118. Ferreira ALO, Giordano RLC, Giordano RC. Nonconventional reactor for enzymatic synthesis of semi-synthetic β-lactam antibiotics. *Ind Eng Chem Res*. 2007;46(23):7695-7702.
119. Ameer GA, Raghavan S, Sasisekharan R, Harmon W, Cooney CL, Langer R. Regional heparinization via simultaneous separation and reaction in a novel Taylor-Couette flow device. *Biotechnol Bioeng*. 1999;63(5):618-624.
120. Hubacz R, Ohmura N, Dluska E. Intensification of starch processing using apparatus with Couette-Taylor flow. *J Food Process Eng*. 2013; 36(6):774-785.
121. Masuda H, Horie T, Hubacz R, Ohmura N. Process intensification of continuous starch hydrolysis with a Couette-Taylor flow reactor. *Chem Eng Res Des*. 2013;91(11):2259-2264.
122. Haut B, Ben Amor H, Coulon L, Jacquet A, Halloin V. Hydrodynamics and mass transfer in a Couette–Taylor bioreactor for the culture of animal cells. *Chem Eng Sci*. 2003;58(3–6):777-784.
123. Zhu XH, Arifin DY, Khoo BH, Hua J, Wang C-H. Study of cell seeding on porous poly(d,l-lactic-co-glycolic acid) sponge and growth in a Couette–Taylor bioreactor. *Chem Eng Sci*. 2010;65(6): 2108-2117.
124. Pal A, Khakhar DV. Breakage of vesicles in a simple shear flow. *Soft Matter*. 2019;15(9):1979-1987.
125. Liu Z, Jin T, Kind M. Continuous polymerization of methyl methacrylate in a Taylor-couette reactor. I. Influence of fluid dynamics on monomer conversion. *Polym Eng Sci*. 2013;53(1):96-104.
126. Woliński J, Wroński S. Interfacial polycondensation of polyarylate in Taylor-Couette-reactor. *Chem Eng Process Process Intensif*. 2009;48 (5):1061-1071.
127. Oberhoff M, Jung WA, Hagemeister E, Heimeier U, Inventors; BASF, assignee. Kontinuierliches Polymerisationsverfahren zur Erzeugung von Polymeren mit enger Molmassenverteilung und Taylor-Couette-Reaktor für seine Durchführung 2007.
128. Liu Z, Kind M. Continuous polymerization of methyl methacrylate in a Taylor-couette reactor. II. Influence of fluid dynamics on polymer properties. *Polym Eng Sci*. 2013;53(5):950-955.
129. Kádár R, Liu Z, Kind M, Bălan C. Influence of hydrodynamic activation on a polymerization reaction in a Taylor-couette reactor. *UPB Sci Bull Ser D: Mechan Eng*. 2010;72(3):149-156.
130. Liu Z, Kádár R, Kind M. Hydrodynamic activation of the batch-polymerization of methyl methacrylate in a Taylor-Couette reactor. *Macromol Symp*. 2011;302(1):169-178.
131. Imamura T, Saito K, Ishikura S, Nomura M. A new approach to continuous emulsion polymerization. *Polym Int*. 1993;30(2):203-206.
132. Kataoka K, Ohmura N, Kouzu M, Simamura Y, Okubo M. Emulsion polymerization of styrene in a continuous Taylor vortex flow reactor. *Chem Eng Sci*. 1995;50(9):1409-1416.
133. Wei X, Takahashi H, Sato S, Nomura M. Continuous emulsion polymerization of styrene in a single Couette-Taylor vortex flow reactor. *J Appl Polym Sci*. 2001;80(11):1931-1942.
134. Rüttgers D, Negoita I, Pauer W, Moritz H-U. Process intensification of emulsion polymerization in the ContinuousTaylor reactor. *Macromol Symp*. 2007;259(1):26-31.
135. Xue W, Yoshikawa K, Oshima A, Sato S, Nomura M. Continuous emulsion polymerization of vinyl acetate. II operation in a single Couette-Taylor vortex flow reactor using sodium lauryl sulfate as emulsifier. *J Appl Polym Sci*. 2002;86(11):2755-2762.
136. González G, Colmenar E, Diaconu G, et al. Production of widely different dispersed polymers in a continuous Taylor-Couette reactor. *Macromol React Eng*. 2009;3(5–6):233-240.
137. Kim M, Park KJ, Lee KU, et al. Preparation of black pigment with the Couette–Taylor vortex for electrophoretic displays. *Chem Eng Sci*. 2014;119:245-250.
138. Kang SH, Lee SG, Jung WM, et al. Effect of Taylor vortices on calcium carbonate crystallization by gas–liquid reaction. *J Cryst Growth*. 2003;254(1):196-205.
139. Jung W-M, Hoon Kang S, Kim K-S, Kim W-S, Kyun CC. Precipitation of calcium carbonate particles by gas–liquid reaction: morphology and size distribution of particles in Couette-Taylor and stirred tank reactors. *J Cryst Growth*. 2010;312(22):3331-3339.
140. Jung T, Kim W-S, Choi CK. Effect of nonstoichiometry on reaction crystallization of calcium carbonate in a Couette−Taylor reactor. *Cryst Growth Des*. 2004;4(3):491-495.
141. Jung T, Kim W-S, Choi CK. Effect of monovalent salts on morphology of calcium carbonate crystallized in Couette-Taylor reactor. *Cryst Res Technol*. 2005;40(6):586-592.
142. Aljishi MF, Ruo AC, Park JH, Nasser B, Kim WS, Joo YL. Effect of flow structure at the onset of instability on barium sulfate precipitation in Taylor-Couette crystallizers. *J Cryst Growth*. 2013; 373:20-31.
143. Nguyen AT, Kim JM, Chang SM, Kim WS. Taylor vortex effect on phase transformation of guanosine 5-monophosphate in drowning-out crystallization. *Ind Eng Chem Res*. 2010;49(10):4865-4872.
144. Jung JY, Lee JG, Baek YK, Kim YD, Hong JP, Kim YK. High throughput process for the continuous preparation of quantum dots using fluid dynamically controlled reactor. *J Alloys Compd*. 2019;784: 816-821.
145. AlAmer M, Lim AR, Joo YL. Continuous synthesis of structurally uniform graphene oxide materials in a model Taylor-Couette flow reactor. *Ind Eng Chem Res*. 2019;58(3):1167-1176.
146. Park WK, Kim H, Kim T, et al. Facile synthesis of graphene oxide in a Couette-Taylor flow reactor. *Carbon*. 2015;83:217-223.
147. Hong SB, Jeong JM, Kang HG, et al. Fast and scalable hydrodynamic synthesis of MnO2/defect-free graphene nanocomposites with high rate capability and long cycle life. *ACS Appl Mater Interfaces*. 2018; 10(41):35250-35259.
148. Jeong JM, Jin SB, Yoon JH, et al. High-throughput production of heterogeneous RuO2/graphene catalyst in a hydrodynamic reactor for selective alcohol oxidation. *Catalysts*. 2019;9(1):25.
149. Lee SE, Park SH. Enhanced dispersion and material properties of multi-walled carbon nanotube composites through turbulent Taylor-Couette flow. *Compos Part A*. 2017;95:118-124.
150. Yu W, Gregory J, Campos LC. Breakage and re-growth of flocs: effect of additional doses of coagulant species. *Water Res*. 2011;45 (20):6718-6724.
151. Vlieghe M, Coufort-Saudejaud C, Frances C, Line A. In situ characterization of floc morphology by image analysis in a turbulent Taylor-Couette reactor. *AIChE J*. 2014;60(7):2389-2403.
152. Metaxas A, Wilkinson N, Raethke E, Dutcher CS. In situ polymer flocculation and growth in Taylor- Couette flows. *Soft Matter*. 2018; 14(42):8627-8635.
153. Weaver JE, Hong H, Ducoste JJ, de los Reyes FL. Controlling aerobic biological floc size using Couette-Taylor bioreactors. *Water Res*. 2018;147:177-183.

**How to cite this article:** Schrimpf M, Esteban J, Warmeling H, Färber T, Behr A, Vorholt AJ. Taylor-Couette reactor: Principles, design, and applications. *AIChE J*. 2021;67:e17228. https://doi.org/10.1002/aic.17228

15475905, 2021, 5, Downloaded from https://aiche.onlinelibrary.wiley.com/doi/10.1002/aic.17228, Wiley Online Library on [09/07/2024]. See the Terms and Conditions (https://onlinelibrary.wiley.com/terms-and-conditions) on Wiley Online Library for rules of use; OA articles are governed by the applicable Creative Commons License